INFILTRATION RATE AND HYDRAULIC CONDUCTIVITY OF SAND-SILT SOILS IN THE PIEDMONT PHYSIOGRAPHIC PROVINCE

A Thesis
Presented to
The Academic Faculty

by

William Randall Pettyjohn Jr

In Partial Fulfillment
of the Requirements for the Degree
Master of Science in the
School of Civil and Environmental Engineering

Georgia Institute of Technology
December 2014

INFILTRATION RATE AND HYDRAULIC CONDUCTIVITY OF SAND-SILT SOILS IN THE PIEDMONT PHYSIOGRAPHIC PROVINCE

Approved by:

Dr. Susan Burns, Advisor
School of Civil and Environmental Engineering
Georgia Institute of Technology

Dr. J. David Frost
School of Civil and Environmental Engineering
Georgia Institute of Technology

Dr. J. Carlos Santamarina
School of Civil and Environmental Engineering
Georgia Institute of Technology

Date Approved: August 21, 2014

“Wonder is the desire for knowledge” Saint Thomas Aquinas

ACKNOWLEDGEMENTS

I would like to thank my advisor, Dr. Susan Burns, for being my inspiration to pursue this research. Dr. Burns' love of the subject and gift for teaching sparked my curiosity in geotechnical engineering, and I will forever be grateful. I would like to thank the committee, including Dr. Frost and Dr. Santamarina, for their time and thoughtful considerations. I hold the three of you in the highest regard and can only aspire to one day be as knowledgeable and gracious.

I would like to thank Georgia Department of Transpiration, who provided the opportunity for me to pursue this research, in particular Jon Griffith for his guidance with the project.

I would like to thank the Geoenvironmental Group, in particular Kip Gray and Nicole Caruso. Kip spent countless hours helping me in the lab, and Nicole volunteered entire days for field work, both of their own accord.

I would like to acknowledge the entire Geosystems group. You are collectively the nicest, most sincere group of people I have ever known. Each of you has contributed to my education and overall experience in some way.

I would like to thank my parents, Randy and Kathy, and sisters, Arica and Cortney, for their love and continued support throughout my life.

Lastly, I would like to thank my wife and best friend, Lindsey Pettyjohn, for her unending support and encouragement throughout my time at Georgia Tech.

TABLE OF CONTENTS

LIST OF TABLES

LIST OF FIGURES

SUMMARY

In this study, a two phase investigation of the hydraulic conductivity parameters of silty soils was performed. In the first phase, double-ring infiltrometer tests were used to measure infiltration rates in-situ at two sites in the Piedmont physiographic province of Georgia. The efficacy of predicting saturated hydraulic conductivity for Piedmont soils via published soil surveys from the National Resource Conservation Service and pedotransfer functions was then investigated. Work focused on the development of a consistent test methodology for soils (sandy, to silts and clays) in the Piedmont, and the final test method utilized being the constant head test, using a double-ring infiltrometer with Mariotte tubes to maintain the head.

In the second phase of the investigation, laboratory based measurements of the saturated hydraulic conductivity of binary mixtures of fine sand and nonplastic silt were performed to investigate the effects of particle mixtures on hydraulic conductivity. The materials used were ASTM 100/200 sand and Sil-Co-Sil 40 non-plastic silt, chosen based on the ratio of the mean particle diameters. Significant effort was invested in the development and comparison of methodologies to produce uniform specimens of the binary mixtures for hydraulic conductivity testing, with the final being modified dry tubing. Two fixed densities were used to investigate the effects of particle packing on the hydraulic conductivity of binary mixtures, with critical fines contents chosen to ensure the finer particles primarily filled the pore volume of the coarse particles. Incremental fines contents, by mass, up to this theoretical fines content were tested. The measured saturated hydraulic conductivity was evaluated in terms of fines content, global and

intergranular void ratio, and confining stress. Models for predicting extreme void ratios and saturated hydraulic conductivity of binary mixtures were also investigated.

The major findings of this study include:

- Predicted values from the NRCS over predicted every measured value of in-situ saturated hydraulic conductivity.
- Predicted values from the ROSETTA pedotransfer software (based primarily on soil grain size) more closely predicted the saturated hydraulic conductivity of the Piedmont soils.
- Saturated hydraulic conductivity of the sand/silt mixture decreased precipitously (by two orders of magnitude) with the introduction of the silt up to the estimated critical fines content of 17%.
- The rate of decrease of hydraulic conductivity decreased when the fines content was above the critical fines content of the binary mixture.
- Decreases in saturated hydraulic conductivity with increasing density, or decreasing global void ratio, were greater in specimens containing more than 1% silt.
- The saturated hydraulic conductivity decreased with decreasing global void ratio and increasing intergranular void ratio.
- Predictive models for extreme void ratios of binary mixtures consistently under predicted the measured void ratios.
- Predictive models for saturated hydraulic conductivity consistently over predicted measured rates.

Chapter 1

INTRODUCTION

Urbanization is typically accompanied by significant increases in the level of surfaces that are relatively impervious to rainfall. As a result, as stormwater runoff flows over low permeability surfaces, such as paved streets and highways, lawns, roofs, and any other surfaces disturbed by human activity, it accumulates chemicals, debris, and solid particles, often referred to as total suspended solids or TSS, as well as a variety of biological contaminants. Consequently, interest in researching differing methods to efficiently and economically treat stormwater runoff has increased over the past decades. In the past, stormwater runoff was considered a nuisance to be dealt with using detention facilities (WEF et al. 2012). However, a recent shift in thinking has led to viewing stormwater runoff as a potential resource to be returned to groundwater and ultimately filtered back to receiving waterways. This shift in the approach of stormwater treatment is the basis for low-impact development, or the practice of construction methods and stormwater best management practices (BMPs) that limit the impacts on natural water flows and cycles (WEF et al. 2012), such as infiltration trenches and ponds.

The ASCE (2012) Manual of Practice (MOP) defines an infiltration BMP as a stormwater BMP that treats the design volume by allowing water infiltration into native soil and into shallow aquifers where it can then make its way into receiving streams. Infiltration BMPs typically consist of a layer of gravel or coarse sand to store the capture volume, overlaying the native soil (Figure 1-1).

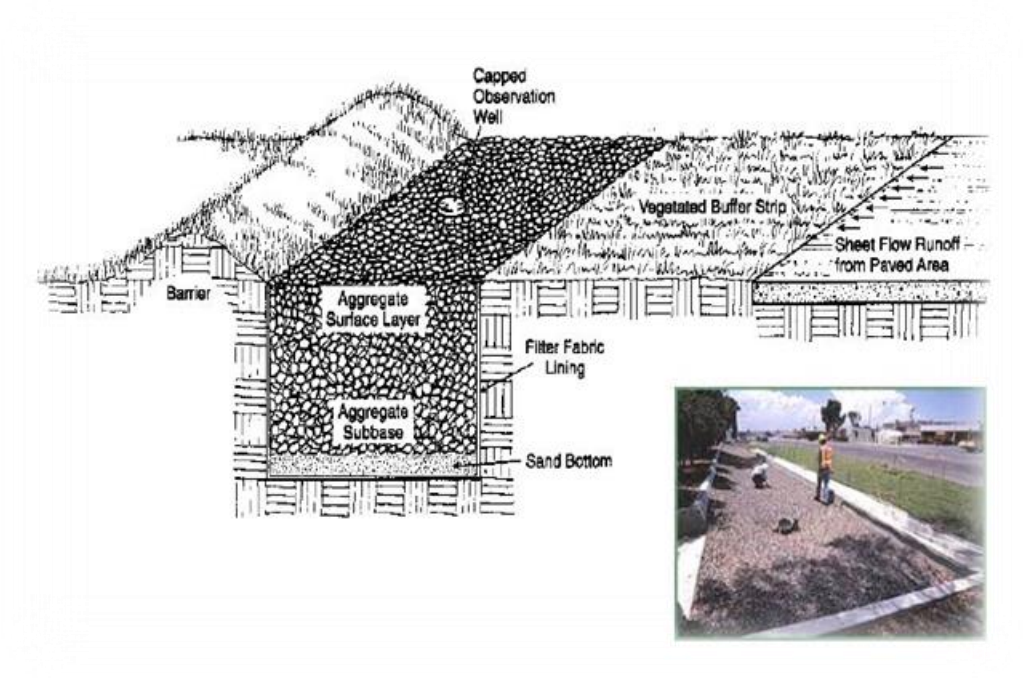

Figure 1-1 The cross section of a generic infiltration trench is shown. Figure from Georgia Stormwater Manuel Volume 2

Currently, infiltration trenches are designed with a vegetated buffer to enhance sedimentation and filtration, with the goal of reducing the quantity of suspended solids in the stormwater runoff before it enters the trench. The aim is to reduce the solids loading in order to slow the rate of clogging of the coarse fill in the infiltration trench. Additionally, geotextiles are used to establish a filter layer, in order to further reduce clogging.

The essential information needed to estimate infiltration rates includes the hydraulic parameters of the in-situ soil, with the soil type and saturated hydraulic conductivity being the two most basic pieces of information required. While the hydraulic conductivity and infiltration rate are not synonymous, the hydraulic

conductivity is the parameter most commonly referred to when evaluating rates for infiltration BMPs. The hydraulic conductivity of a soil depends on the viscous drag on the fluid by the particle surfaces (Santamarina et al. 2001). As the pore space is filled with finer particles the volume available for fluid conduction decreases and the surface area, that contributes to viscous drag, increases. There are inherent challenges in determining the saturated hydraulic conductivity of a soil. In-situ measurements of hydraulic conductivity have been shown to have coefficients of variation as high as 400% (Reynolds et al. 2002). Geotechnical grain size and index parameters can be used to estimate an order of magnitude range of hydraulic conductivity, using correlations to estimate hydraulic conductivity or tabular values of hydraulic parameters based on the soil classification; however, unsaturated parameters are required for many of the classical infiltration rate equations, including air entry pressure, water content at saturation, and residual water content, which are required to estimate the effects of capillarity on the infiltration rate before saturation is achieved.

Multiple parameters influence the hydraulic conductivity of soils, including the relative size ratio of particles within the mixture. For example, increased soil densities are obtained with the introduction of smaller grains into a matrix of larger grains. If the density, or void ratio, of the large particles is held constant, the addition of smaller particles will increase the global density of the mixture, which is a function of the particle size ratio between the individual constituents of the mixture (McGeary 1961). At a critical value of smaller particles, the voids of the larger particles will be filled, and at this critical value the larger particles are essentially floating in a matrix of smaller particles. This represents a transition at which the behavior of the global mixture changes from

being dominated by the characteristics of the larger particles to that of the smaller particles. This critical value of smaller particles, or fines, has been studied extensively in geotechnical engineering in terms of strength parameters and liquefaction; however, there are relatively fewer studies available on its impact on hydraulic conductivity. The hydraulic conductivity of particle mixtures impacts engineering behavior of groundwater transport, mining applications, slurry walls, and filter media.

Obtaining these hydraulic parameters economically is a challenge due to the extensive testing required for both saturated and unsaturated soils. Consequently, in practice, the required parameters typically are first estimated based on known characteristics of the soils in the area. As the project proceeds, in-situ or lab tests are then performed to validate the estimations. This two-pronged approach is found in municipal stormwater manuals and recent publications by the WEF and ASCE. The hydraulic parameters required can be obtained in the following order (Massman 2003; WEF et al. 2012): first: obtain estimates by referencing published soils data or historical site information, and second, if the estimate is greater than minimum rate allowed follow up with in-situ or lab testing to confirm site feasibility. The minimum acceptable rate for infiltration is determined by local municipalities, with values varying as a function of regional geography (Table 1-1). The additional design steps are carried out once the rate is measured and the feasibility of the site for construction is determined.

Table 1-1 Minimum Saturated Hydraulic Conductivity Values for Infiltration BMPs

Minimum Infiltration Rate (in/hr)	Organization
0.5	Atlanta (Georgia) Regional Commission
0.2	Minnesota Pollution Control Agency
0.1	Pennsylvania Department of Environmental Protection
0.4	ASCE / WEF

Good design requires review of the methods for estimation of conductivity parameters, as well as review of the measurement techniques that are available in practice today. In addition, it is of fundamental importance to ensure a solid scientific understanding of the infiltration process. Consequently, this thesis will begin with a review of the fundamentals that are critical to successful design of infiltration BMPs. Next, infiltration rates were measured at field sites in the Piedmont physiographic region of Georgia using a double-ring infiltrometer. Field measured values were compared with published soils data from the USDA Soil Survey database and predicted values via pedotransfer functions. Finally, the saturated hydraulic conductivity of a sand-silt binary mixture was experimentally quantified at the lab scale. Effects of increasing silt contents and the subsequent changes in global and intergranular void ratios on saturated hydraulic

conductivity were examined. The effect of confining pressure on the measured hydraulic conductivity and models to predict the saturated hydraulic conductivity were also studied.

Chapter 2

LITERATURE REVIEW

2.1 Unsaturated Flow

Most commonly in infiltration BMPs, the infiltration of water occurs when the filter media and fill soils are not fully saturated (Barbu and Ballestero 2014). Consequently, the initial infiltration period is governed by the influence of capillarity on early time infiltration rates. Capillarity is influenced by the surface tension of the fluid, as well as the contact properties of the solid and the liquid. To illustrate the phenomena of surface tension, a vapor-water interface can be considered: water molecules in the liquid state are polar, and are attracted to each other through van der Waals forces. The van der Waals forces felt between the water molecules within the liquid are isotropic because the molecules are surrounded by water molecules on all sides. However, molecules within approximately five to ten monolayers of the interface between the vapor and the liquid phases have unbalanced forces acting due to the absence of liquid water on all sides. Consequently, these molecules orient with their negative side toward the vapor, resulting in an unbalanced van der Waals attraction along the interface (Lu and Likos 2004; Santamarina and Jang 2010). This phenomena results in a contractile membrane along the interface, which produces a measureable surface tension, T_S (Santamarina and Jang 2010).

In the case of a solid-liquid interface, there is a tendency to contract due to the interfacial tension between the materials (Santamarina and Jang 2010). The angle produced at the interface of the liquid and the solid phase is defined as the contact angle.

The degree of this angle depends on the mineral composition and surface charge of the particle, and its tendency to attract (wetting) or repel (nonwetting) the fluid. The contact angle has an important influence on the geometry of interface contacts and physical behavior of the system (Lu and Likos 2004), and most mineral surfaces are considered water-wet (Santamarina and Jang 2010).

Capillary rise in an idealized cylinder with a wetting contact angle ($\alpha < 90^{o}$) can be defined as follows (Figure 2-1):

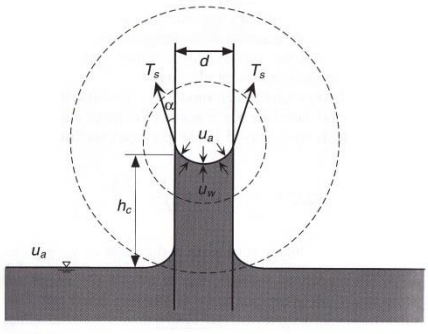

Figure 2-1 A cylinder is used as an example to illustrate capillary rise. Figure from Lu and Likos 2004.

$$\gamma_w h_c \pi r^2 = 2\pi r T_S \cos\alpha$$

$$\rightarrow h_c = \frac{2}{r\gamma_w} T_S \cos\alpha$$

where γ_w = unit weight of water, h_c = height of the capillary rise, r = radius of the cylinder, T_s = surface tension, and α = contact angle (Santamarina et al. 2001). The water-vapor interface can also be described as the pressure difference between the vapor and water phase.

As water dries or evaporates from soils, the curvature of the water-vapor interface begins to curve as a result of the pressure difference between the water-vapor phase. This pressure difference is dependent on the curvature of the interface and the surface tension,

T_S (Cho and Santamarina 2001). The curvature of the interface can be characterized by the radii r_1 and r_2 as defined by the Laplace equation:

$$(u_a - u_w) = T_S\left(\frac{1}{r_1} + \frac{1}{r_2}\right)$$

This pressure difference is referred to as matric suction and is typically referenced with the variable ψ.

As water drains or evaporates from soils, the menisci at the particle-pore fluid boundaries pull inward to become more convex (Cho and Santamarina 2001). The classifications of the particle-pore fluid bridges for different meniscus configurations are known as the pendular, funicular, and capillary phases. These can be observed in order of increasing saturation, respectively (Urso et al. 1999).

For an initially saturated soil, the pressure required for air to enter the void space is referred to as the air entry pressure, ψ_{ae}. The air entry pressure is dependent on the radius of the pore openings and on the grain size of the soil, and is higher as the pore size decreases. Consequently, air entry values are much higher for clays and silts than for sands and gravels (Cho and Santamarina 2001; Lu and Likos 2004). The air entry phase typically occurs during the capillary phase, in which the bulk soil is still primarily saturated and capillary bridges occur between particles (Urso et al. 1999).

The funicular phase is defined when the air has entered the pore space but the water is still in a continuous phase. The drying rate is relatively constant during the funicular phase (Cho and Santamarina 2001). The change in radius of the menisci relative to the capillary phase is small, thus the matric suction in this phase is moderate with regard to the Laplace equation (Cho and Santamarina 2001).

The pendular phase begins once the water bridges between particles begin to disconnect (Cho and Santamarina 2001; Urso et al. 1999). Pore water in this phase consists primarily of that adsorbed to particle surfaces (Lu and Likos 2004). The radius of the menisci relative to the capillary and funicular phases is small, thus matric suction is high with regard to the Laplace equation (Cho and Santamarina 2001). Meniscus geometry for coarse grained particles exhibiting the capillary, funicular, and pendular bridges shows distinct structure as a function of water content (Figure 2-2).

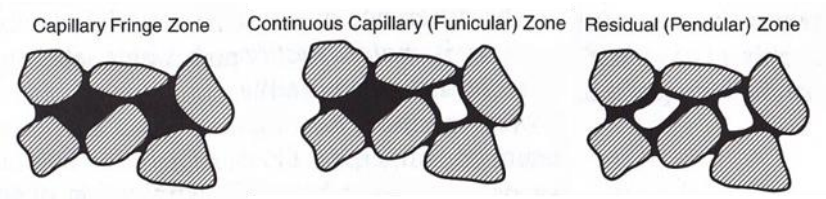

Figure 2-2 Saturation phases are shown. From left to right the saturation phases represented are the capillary, funicular, and pendular phases. Figure from Lu and Likos 2004.

The constitutive relationship between soil water content, or degree of saturation, and matric suction is described by the soil water characteristic curve (SWCC). A SWCC is typically displayed with a semi-log scale that organizes three different phases of water content: the tightly adsorbed, adsorbed film, and "capillary" phase (Figure 2-3) (Lu and Likos 2004). These water content descriptions implicitly correspond to the saturation stages and corresponding pore fluid menisci.

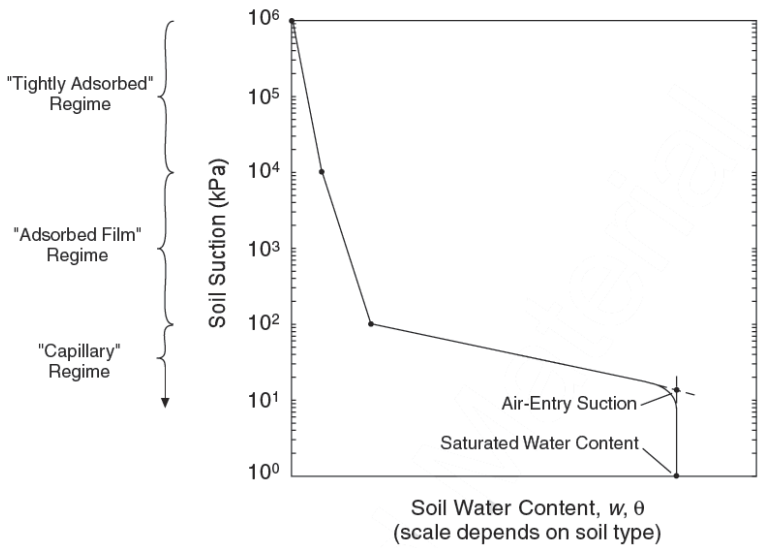

Figure 2-3 The SWCC curve is shown for a generic soil. The capillary, adsorbed, and tightly adsorbed regimes correspond with the aforementioned saturation phases. Figure from Lu and Likos 2004.

The water content corresponding to the magnitude of matric suction varies between the wetting and drying phase. There are many theories relating this hysteresis to both micro and macro scale phenomena (Lu and Likos 2004). Some examples include hysteresis in contact angle between pore fluid and particles during wetting and drying, swelling and shrinking of fine grained soils during wetting and drying, and nonhomogeneous pore size distribution, or the "ink-bottle" effect (Lu and Likos 2004).

Measurement techniques for matric suction most commonly involve the use of tensiometers in the field, and pore water extraction tests using a pressure plate apparatus in the lab. ASTM D6836 offers guidance in selecting the appropriate apparatus based on the soil type being tested. Methods using a centrifuge have also been proposed to increase the speed of obtaining the parameters necessary to measure the SWCC (Zornberg et al. 2010).

There are numerous models relating matric suction to water content. One of the most commonly implemented models was proposed by van Genuchten (1980):

$$\theta = \theta_r + \frac{\phi - \theta_r}{\left[1 + \left(\frac{\psi}{\psi_{ae}}\right)^n\right]^{1-\frac{1}{n}}} = \theta_r + \frac{\phi - \theta_r}{[1 + (\alpha\psi)^n]^m}$$

where ψ = matric suction, ψ_{ae} = air entry pressure, Φ = porosity, θ = water content, and θ_r = residual water content. The variable n is a function of grain size distribution and m = 1 – 1/n. The van Genuchten parameters can be fit to experimental values of matric suction measured in the lab, estimated by grain size distribution using one of many proposed pedotransfer functions (PTFs), or referenced in tabulated values by soil type.

The result of matric suction on the infiltration process is that water is pulled by the matric suction of the drier soils, in addition to gravity flow from the ponded water (Ferguson 1994). This combined driving gradient can be explained using Darcy's law by combining the matric suction into the total head:

$$q_z = -K\frac{dh_t}{dz}$$

The terms q_z = flow rate through a given cross sectional area of soil in the vertical (z) direction, K = coefficient of hydraulic conductivity, and h_t = total head. As discussed previously, the total head in unsaturated flow is a function of both gravity flow and matric suction. Buckingham (1907) modified this form of Darcy's equation to represent unsaturated flow:

$$q_z = -K(\theta)\left[1 + \frac{d\psi(\theta)}{dz}\right]$$

Evaluating Darcy's law for unsaturated conditions, it can be seen that one dimensional flow for unsaturated conditions is a function of both gravity flow and matric suction. The degree of matric suction depends on the water content of the soil and the soil type.

Richard's equation is obtained by taking the derivative of the above equation for one dimensional flow, with respect to the z-direction, and combining Darcy's law and the conservation of mass. Richard's equation is the basic theoretical equation describing infiltration of water into a homogenous soil mass (Dingman 2008). The one dimensional version of Richards's equation is expressed below as follows:

$$-\frac{\partial \mathrm{K}(\theta)}{\partial \mathrm{z}}+\frac{\partial}{\partial \mathrm{z}}\left[\partial \mathrm{K}(\theta)\frac{\partial \psi(\theta)}{\partial \mathrm{z}}\right]=\frac{\partial \theta}{\partial \mathrm{t}}$$

Richard's equation is non-linear, without closed form analytical solutions; however, it can be used for numerical modeling of infiltration by applying boundary conditions, initial conditions and then solving the equation for thin layers for small time changes (Dingman 2008).

2.2 Infiltration Models

Due to the complexity of the forces governing hydraulic conductivity, many approximate solutions have been developed to obtain closed form solutions for infiltration rates. The Horton equation is an empirical model used in practice by stormwater designers (Ferguson 1994), which is expressed simply in terms of initial infiltration rate (f_0), final infiltration rate (f_p), time, and an empirical constant, k:

$$f(t) = f_p + \left(f_o - f_p\right)^{-kt}$$

It is typically considered that f_p approaches k_{sat} at steady state infiltration rates. The benefit of using the Horton equation is its simplicity. It is easily fitted to experimental data; however, the Horton equation is purely empirical and has no physical

basis. Closed form analytical solutions are often needed for inclusion in hydrologic models (Dingman 2008; Lu and Likos 2004), which is one of the motivations for developing empirical models.

The Green and Ampt model (1911) assumes a sharp, uniformly propagating wetting front (z_f), constant water contents above (Φ) and below (θo) the wetting front, and that the matric suction directly under the wetting front (ψ_f) is greater than the ponded water height (H) (Dingman 2008; Ferguson 1994; Lu and Likos 2004). Given cumulative infiltration (F(t)) as an input parameter, a non-linear expression can be solved iteratively to determine a value of ψ_f (Dingman 2008).

$$ln\left(1 - \frac{F(t)}{(\phi - \theta_o)\psi_f}\right) = \frac{K_{sat}t - F(t)}{(\phi - \theta_o)\psi_f}$$

The depth of the wetting front (z_f) and infiltration rate can then be solved.

$$z_f = \frac{F(t)}{(\phi - \theta_o)}$$

The Philip model offers a simplified solution to Richards equation based on an infinite series solution for ponded water infiltrating into a indefinitely deep soil (Dingman 2008; Lu and Likos 2004):

$$f(t) = \frac{S_p}{2}t^{-\frac{1}{2}} + A_2 + A_3\,t^{\frac{1}{2}} + A_4 t + \cdots + A_n{}^{\frac{n}{2-1}}$$

Typically, only the first two terms are considered and A_2 is treated as k_{sat}, or the final infiltration rate:

$$f(t) = \frac{S_p}{2}t^{-\frac{1}{2}} + K_p$$

The terms K_P and S_p are the final infiltration rate, and sorptivity, defined as:

$$S_p = \left[(\phi - \theta_o)K_{sat}|\psi_{AE}|\left(\frac{2b+3}{b+3}\right)\right]^{\frac{1}{2}}$$

The term b is a constant related to the grain size distribution, and ψ_{ae} is obtained from the SWCC. It is common practice to estimate S_p and K_p as empirical parameters by fitting the values to measured infiltrometer data. The model works particularly well with the spatial variability of infiltrometer data (Dingman 2008; Ferguson 1994).

Practitioners commonly use tabulated input parameters by soil type to make initial estimates of infiltration rates (Ferguson 1994). Rawls et al. (1983) and Rawls et al. (1982) have developed tables based on soil type that provide input parameters specifically for the Green-Ampt equation and SWCC, respectively.

Table 2-1 summarizes the aforementioned infiltration models and summarizes their respective advantages, disadvantages and required input parameters (Bedient et al. 2013; Dingman 2008; Ferguson 1994; Lu and Likos 2004).

Table 2-1 Summary of Three Commonly Used Infiltration Rate Equations

Model	Assumptions	Input Parameters	Advantages	Disadvantages
Green-Ampt (1911)	Uniform wetting front	k_{sat}, porosity, initial water content, cumulative infiltration	Few input variables required	Cumulative infiltration required input parameter
Horton (1940)	Empirical	Based on measured data	Simple	Empirical
Philip (1957)	Smooth wetting front	k_{sat}, air entry pressure, b, porosity, initial water content	Predicts cumulative infiltration, works well with infiltrometer data	Does not theoretically hold for time approaching zero and infinity, many input parameters required

These three models represent the ones applied most frequently in literature, textbooks, and design manuals from professional practice. All three models provide a similar fit to the data when compared with numerical solutions based on Richard's equation, assuming a constant water supply (Hsu et al. 2002). There are numerous infiltration models in the literature and in practice, and a review of additional infiltration models can be found in EPA report EPA/600/R-97/128b (Chen et al. 1998).

2.3 Rate Determination

It has been shown that the infiltration rate is a controlled by both capillarity and saturated hydraulic conductivity. However, saturated hydraulic conductivity alone is the most often used parameter for the design rate for infiltration BMPs (WEF et al. 2012). This design approach neglects the unsaturated phase, which is a conservative approach because the saturated infiltration rate is always slower than the unsaturated rate of infiltration (Massman 2003). Despite this widespread practice, the following section will review methods for estimating and measuring both the saturated and unsaturated hydraulic conductivity parameters.

2.3.1 Published Soils Data

Soil Survey data available through USDA-NRCS is a tool used for initial estimates of soil properties. All the historical data from the NRCS soil surveys by county has been digitized and is available via the Web Soil Survey. Estimates of hydraulic conductivity referenced by NRCS data are based on texture and bulk density, but also take into account overriding parameters such as macropore flow (Arrington et al. 2013). The validity of using NRCS data to estimate saturated hydraulic conductivity for stormwater applications has been investigated by Fedler et al., who compared NRCS estimates to measured values for ten counties in the state of Texas. It was found that the

data from NRCS did not correlate with the field measured values (Fedler et al. 2012). Arrington et al. (2013) found that NRCS predicted values had a lower root mean squared error when compared to measured values and values found in tables used by stormwater practitioners (Arrington et al. 2013).

2.3.2 Pedotransfer Functions

Hydraulic properties can also be estimated by pedotransfer functions (PTFs). A PTF references an existing database of measured soil properties. Utilizing this existing database, input parameters such as sand/silt/clay fraction and in-situ density can be used to estimate hydraulic properties (Wösten et al. 2001).

One widely used source is a table based on USDA soil textural classification developed by Rawls et al. (1982). Measured data from 1,323 soils with 5,350 horizons from 32 states were used as a basis (Rawls et al., 1982). Regression analysis was used to estimate the hydraulic properties for the eleven standard USDA soil types. The hydraulic properties included porosity, residual saturation, effective porosity, air entry pressure, pore size distribution, water retained at -0.33 bar and -15 bar, and saturated hydraulic conductivity (Rawls et al., 1982). Saxton et al. (1986) developed a model based on the same data that could estimate additional hydraulic properties by using sand/silt/clay fraction as the only input parameter. Rawls et al. (1992) developed a look-up table that estimated saturated hydraulic conductivity based on USDA soil types (Arrington et al. 2013). This table was updated in 1988 to include soil density and porosity categories as input parameters (Arrington et al. 2013, Rawls et al. 1998). Saxton and Rawls (2006) updated the original model from 1986 to include the updated regression equations from Rawls et al. (1998), organic matter (OM) as an input parameter, and the larger database of the USDA-NRCS soil survey as a reference. This updated model is available in a

software package, Soil-Plant-Atmosphere-Water (SPAW), which is free to download via the USDA Hydrolab.

In addition to hydraulic conductivity, SPAW provides the properties necessary to estimate the SWCC. The estimated SWCC curve can be used to determine parameters for Green – Ampt and Philips equations to estimate the infiltration rate.

The ROSETTA model is another software package developed to predict hydrualic properties. ROSETTA utilizes five PTFs hierarchically to estimate saturated and unsaturated hydaulic conductivity, and estimation of the van Genuchten parameters (Schaap et al. 2001). It is based on neural network analysis that allows uncertainty estimates to be provided, which is useful when no measured values of k_{sat} are avaliable for comparison (Schaap et al. 2001). The data set is composed of 2,134 soil samples from temparate to sub-tropical climates in North America and Europe; of those samples, 1,306 provide saturated hydraulic conductivity values (Schaap et al. 2001).

The validity of using PTFs to estimate hydraulic paratmeters has been investegated for stormwater applications. Values estimated using a PTF, Precision Agriculture-Landscape Modeling System (PALMS), yielded a lower root mean squared error (RMSE) than published values by Rawls et al. (1998), when compared to measured values for a study in Dane County, Wisconsin (Arrington et al. 2013). Values predicted using Saxton et al. were equally higher and lower than 28 measureed values from ten counties in Texas (Fedler et al. 2012).

2.3.3 In-Situ Methods

The aforementioned methods for estimating hydraulic properties of soils are useful for first cut estimates, but these values are based primarily on texture and do not take into account disturbance and site variability. A geotechnical investigation is

necessary to confirm the conditions in-situ are appropriate for infiltration BMPs. Common methods found in stormwater practice and literature include ring infiltrometers (Bouwer 1986; Reynolds et al. 2002, ASTM D3385) and borehole testing (Bouwer and Rice 1976; Brown et al. 1995).

Borehole infiltration tests are widely employed for in-situ measurements of hydraulic conductivity (Reynolds 2013). Bouwer and Rice proposed a method for slug test data analysis when groundwater is encountered in unconfined aquifers (Bouwer and Rice 1976). This method was shown to produce less error than alternative analysis techniques, such as the Hvorslev method (Brown et al. 1995). The United States Bureau of Reclamation (USBR) methods are used in the geology, water management and engineering applications, while borehole permeameter (BP) methods are often used in agricultural and environmental sciences (Reynolds 2013). It has been shown that BP methods provide more accurate results than the USBR method for most scenarios (Reynolds 2013). Borehole tests can be relatively time consuming and expensive when taking into account the boring and casing required. A more economical alternative is a ring infiltrometer.

A ring infiltrometer consists of either a single or double concentric ring configuration. It is driven into the ground in a manner that minimally disturbs the soil, but is deep enough to prevent side-wall leakage. Falling head and constant head tests can then be performed. A concentric ring set up, or double-ring infiltrometers (DRI), is used to mitigate the impact of lateral flow (Reynolds et al. 2002). The measurements from a DRI are taken only from the center ring, with the annular space accounting for the lateral flow. The flow lines beneath a double ring infiltrometer, through the outer annular space,

are vertical and lateral, as opposed to the flow lines below the center ring, which are primarily vertical (Figure 2-4).

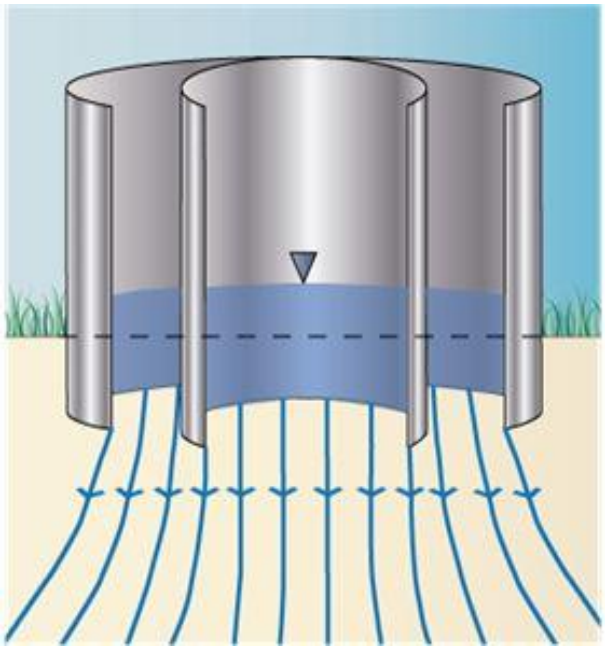

Figure 2-4 A double-ring infiltrometer is shown. The flow lines show the potential for lateral flow around the perimeter of the annular space.

Gregory et al. (2006) performed DRI tests in Northern Florida. Three DRI configurations were evaluated on a residential construction development. An ASTM standard, a Turf-tech 15 and 30 cm DRI with a constant head, and Turf-tech 15 and 30 cm DRI with a falling head were run on a single lot, predevelopment. The differences between the results of the constant head test of the smaller DRI and of the ASTM standard method were not statistically significant. The results of the falling head test with the smaller DRI had an unacceptably high COV (Gregory et al. 2006).

In a study in Auburn, AL, a DRI with 15 and 30 cm rings, similar to the device studied by Gregory et al. (2006), was fitted with a pressure transducer near the bottom of the center ring, and falling head tests were then performed. The results for the modified

DRI were consistently lower than those from results using the ASTM standard method (Arriaga et al. 2010).

It has also been shown that using smaller infiltrometers can yield inaccurate results. Lai and Ren (2007) found that the variability of results decreased with an increase in inner ring diameter, using both numerical and experimental results. The larger center ring allows a better chance of capturing the heterogeneity of the soil and subsequently measuring a more stable hydraulic conductivity. An inner ring diameter of at least 80 cm was recommended (Lai and Ren 2007). The buffer index, the size ratio between the outer and inner rings, was also investigated. It was shown that the buffer index and the inner ring size affect the accuracy of the results. The inner ring size was a more important factor to consider (Lai et al. 2010). The effect of the embedment depth on the accuracy of results was also investigated. Numerical and experimental results from six different outer and inner ring insertion depths show that continuously increasing the depth of insertion would improve the accuracy. But driving the infiltrometer deeper will further disturb the soil and hence affect the accuracy of the results. The authors recommend in insertion depth of between 5 and 15 cm, or approximately the same as is recommended in ASTM D3385 (Lai et al. 2012).

The smaller inner ring diameter has been shown to decrease the accuracy of the results. However, an 80 cm inner ring diameter would be difficult to implement in the field for practical purposes. Of the aforementioned 15/30, 30/60 and larger infiltrometers used in the Lai et al. studies, the 30/60 offers a larger inner ring diameter within a practical size range.

ASTM D3385 recommends running the test for 6 hours or until steady-state values are observed. These steady-state values are then taken as the saturated hydraulic conductivity. This approach does not take into account head due to ponded water, depth of ring insertion, or the ring geometry. Reynolds et al. (2002) proposed a model that takes the aforementioned parameters into account:

$$k_{FS} = \frac{q_s}{\left[\frac{H}{C_1 d + C_2 a}\right] + \left\{\frac{1}{[\alpha(C_1 d + C_2 a)]}\right\} + 1}$$

where the k_{FS} = field saturated hydraulic conductivity, q_s = steady-state flow rate from the DRI, H = height of ponded water, d = diameter of inner ring, a = insertion depth of inner ring, α = macroscopic capillarity length, C_1 and C_2 are empirical constants.

Another method for measuring in-situ hydraulic conductivity is a pilot infiltration test (PIT). A PIT consists of excavating a pit to the depth of the potential BMP, and filling the pit with water to a fixed depth. The test is performed with a constant head, and the amount of water required to maintain the water level is monitored. The technique is based on guidance provided by Massman (2003). The PIT overcomes some of the scaling error inherent in measurements made using a smaller apparatus, such as the DRI. Massman (2003) found that measurements made using the PIT method were on average 50 times lower than estimates provided by Hazen's correlation with D_{10} and regression equations based on grain size distribution. Some of the PIT tests were carried out in existing BMPs, so biofouling or physical clogging could have contributed to the disparity in rates (Massman 2003).

Factors of safety (FS) for measured rates vary. The U.S. EPA suggests using a FS between 25 and 50 (Philips and Kitch 2011). The State of Washington suggests FS

based on the type of soil, and additional considerations such as frequency of inspection and maintenance. The FS range from 5.5 to 18 (Massman 2003). While WEF and ASCE recommend FS between 3.3 and 2, as well as modifiers based on soil type (WEF et al. 2012).

2.4 Southern Piedmont Physiographic Region

The Southern Piedmont physiographic province begins in central Alabama and passes through northern Georgia and continues northeast to the northern tip of Virginia. Metamorphic and igneous rocks from the Precambrian and Paleozoic eras make up the primary bedrock in virtually this entire region (NRCS 2014). The soils in this region are saprolitic, formed from the in-place weathering of this bedrock. The upper portion of the soil is typically classified as silty-fine sand (SM) or low plasticity silt (ML) with less frequent occurrences of clayey sand (SC), sandy clay (SC) and plastic sandy silt (MH) (Finke et al. 2001).

There is limited literature available on stormwater infiltration in the Piedmont region. A study conducted by the U.S. Air Force and the U.S. Atomic Energy Commission (dissolved in 1975) investigated the infiltration of water into basins referred to disposal pits located in Dawson County, Georgia. Rates were measured by continuously pumping water into the basins and maintaining constant heads of one, two, and three feet for several days. The measured infiltration rates ranged from 1.8×10^{-4} – 3.9×10^{-4} cm/s (Stewart 1964).

Ellington and Ferguson (1991) used a computer model from 1990 to simulate the effectiveness of replacing existing detention stormwater BMPs for two sites in the Piedmont region of Georgia. The simulations used data generated for a 50 year storm to show that both sites could use infiltration to reduce peak discharge to below pre-

development levels at a significant cost savings (Ellington and Ferguson 1991). However, only saturated hydraulic conductivity data from published soil maps were used to estimate the final infiltration rates. No lab or in-situ tests were carried out to validate these rates.

Another study monitored the infiltration rates of three BMPs that depended on infiltration in the Charlotte area of North Caroline utilizing three different infiltration BMPs. The BMPs consisted of a pervious pavement, a bio-retention pond and an infiltration basin. Preconstruction infiltration rates were measured using a DRI and subsequent infiltration rates were monitored using pore pressure transducers installed in PVC monitoring wells to measure change in water levels over several months post construction. Preconstruction infiltration rates varied from $1.7 \times 10^{-4} – 2.2 \times 10^{-4}$ cm/s. Post construction rates averaged at 9.9×10^{-5} cm/s. The decrease in post construction rates was attributed to construction activities; i.e. compaction from equipment and clogging of subgrade materials such as gravel and geotextile filters (Estes 2007).

2.5 Binary Mixtures

The classical approach to describing soils in geotechnical engineering is to classify them as sands, silts, or clays; however, soils encountered in the field are commonly mixtures of these soil types. Consequently, the soils typically exhibit particle size distributions that range over several orders of magnitude. There can also be differences in the behavior of the individual constituents of the mixture due to differences in chemical and mechanical properties of minerals. These differences can affect the interparticle interactions and fabric formations of the mixtures (Palomino et al. 2008).

2.5.1 Particle Packing

The two limiting cases of particle packing are simple cubic (maximum void ratio) and cubic tetrahedral packing (minimum void ratio). Figure 2-5 illustrates the largest diameter particle that could theoretically fit in between the larger particles. For the simple cubic and cubic tetrahedral the ratio of the smaller diameter particle to the larger particle diameter is 0.414 and 0.155, respectively (Santamarina et al. 2001). Higher densities can be achieved for binary mixtures with smaller particles sizes that can fit between the larger particles. The density increases, or void ratio decreases, with decreasing particle size ratio, d_s/D_{50} (Santamarina et al. 2001).

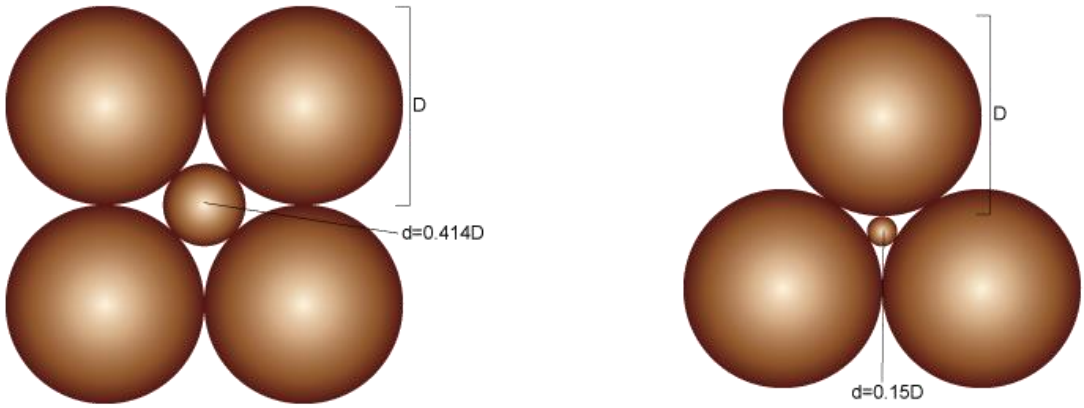

Figure 2-5 The limiting cases for particle packing: simple cubic and cubic tetrahedral. This shows that the maximum ratio of smaller particles contained in the pore space id 0.414 for loose packing and 0.155 for dense packing. Figure adapted from Santamarina et al. 2001.

Furnas (1931) investigated the maximum density of concrete mixtures and determined that mixtures of different particle sizes could increase the density, and that the particle size ratio contributed to this density increase. McGeary (1961) showed that more efficient packing densities could be formed by using mixtures of spheres instead of monosized spheres. It was also shown that the size ratio of the respective spheres could help in increasing packing efficiency. Mixtures of spheres were shown to require a

diameter difference less than seven to measurably increase packing efficiency (McGeary 1961).

McGeary (1961) used glass spheres to obtain ideal packing, and noted that particle shape influenced the maximum and minimum densities, or void ratios, of soils. It has been shown that both the maximum and minimum void ratios decrease as roundness and sphericity increase (Cho et al. 2006). Koltermann and Gorelick (1995) introduced a fractional packing model that accounted for finer material that was not contained within the pore space of the coarser material. The finer particles outside of the pore space of the coarser particles displaced the coarser particles preventing the theoretical densities obtained with ideal packing considerations. It was shown that there were less finer particles retained in the pore space with decreasing particles size ratio (Gorelick and Koltermann 1995).

2.5.2 Critical Fines Content

The increased packing efficiency that can be obtained through the introduction of finer grained particles is limited to a threshold value of finer particles. If ideal packing is assumed, then the addition of finer particles within the void space will increase the density of the global mixture. However, once the voids are completely full, the mixture will reach its theoretical maximum density. Beyond this point, the global characteristics of the mixture reflect that of the finer particles.

This topic was investigated by McGeary (1961) for binary mixtures. Holding the coarser particle size fixed, varying percentages of six different finer particles were introduced into the void space. It was shown that the maximum experimental density of the mixture was achieved at fines contents between 20 and 40 %. The percentage of fines required to achieve the maximum density decreased with decreasing particle size of the

finer material (Figure 2-6) (McGeary 1961). Lade et al. (1998) investigated the minimum and maximum void ratios of fine sands mixed with non-plastic silts. They observed a minimum void ratio of the mixture between fines contents of 20 and 50% for both minimum and maximum void ratios (Lade et al. 1998). This transitional, or threshold, value was implicitly shown by past researchers, and more recent studies have explicitly defined this term.

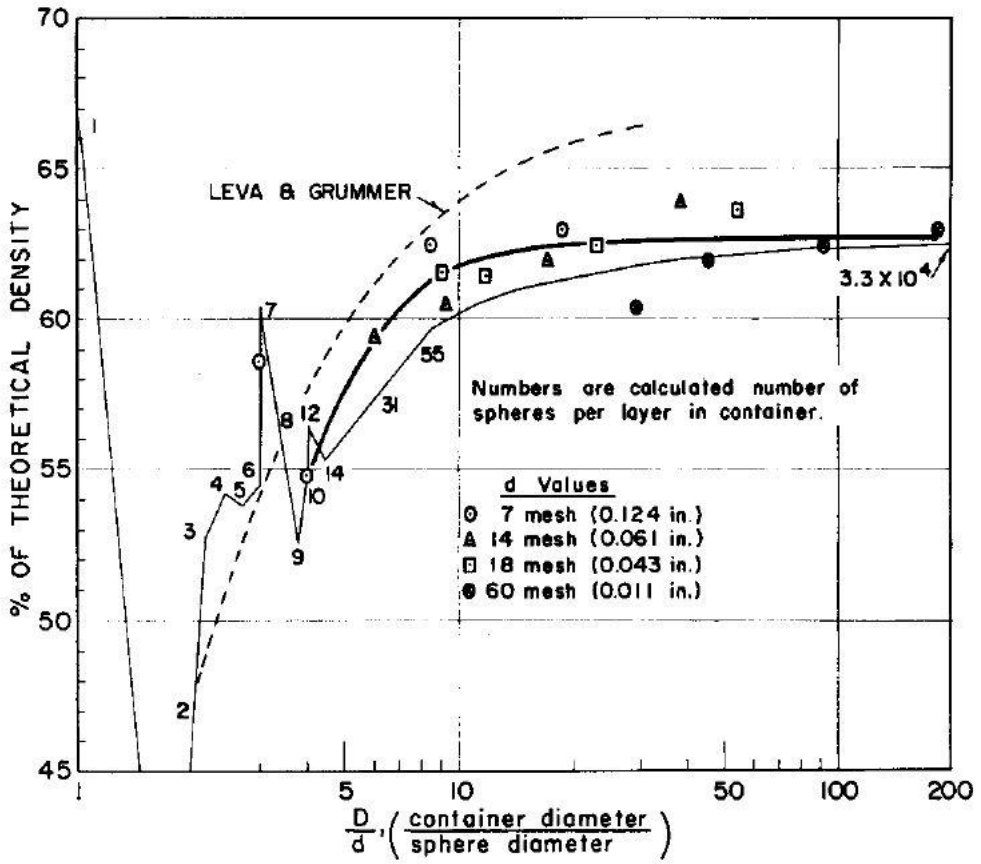

Figure 2-6 Theoretical lower bound densities of binary mixtures are shown as a function of particle size ratio. Figure from McGeary 1961.

The concepts of intergranular and interfine void ratio were defined by Thevanayagam (1998). To investigate strength parameters of binary mixtures,

Thevanayagam assumed that below a threshold value, the fines did not participate in the transfer of forces through particle contacts. The intergranular void ratio was defined as:

$$e_s = \frac{e + FC}{1 - FC}$$

with e = global void ratio, e_s = intergranular void ratio, and FC = fines content. For the purposes of this definition, the fines are assumed to be part of the void space, or "apparent void space" (Thevanayagam 1998).

At some critical value of FC, the global behavior of the mixture is assumed to behave like the finer material. For this scenario, Thevanayagam (1998) defined the interfine void ratio:

$$e_f = \frac{e}{\left(\frac{FC}{100}\right)}$$

The fines content where behavior of the mixture changes from that of the coarser grained to the finer grained component has been defined differently according to different researchers. Thevanayagam et al. (2002) defined it as the "threshold fines content", while Yang et al. (2006) defined this value of fines as the "transitional fines content". Choo and Burns (2014) defined the critical fines content as:

$$FC^* = \frac{G_{sS} \cdot e_L}{G_{sL}(1 + e_s) + G_{sS} \cdot e_L}$$

where G_{sS} = specific gravity of small particles, G_{sL} = specific gravity of large particles, e_L and e_S are the, void ratio of large particles and void ratio of small particles, respectively. If the specific gravities of the larger and small particles are equal, then the expression reduces to (Choo and Burns 2014):

$$FC^* = \frac{e_L}{1 + e_s + e_L}$$

This equation can be used to predict the FC* of mixtures depending on the initial void ratios of the individual constituents. The limiting cases of this equation are:

1. The void ratio of the coarse grained component approaches the minimum void ratio while the fine grained component approaches the maximum void ratio
2. The void ratio of the coarse grained material approaches the maximum void ratio while the fine grained component approaches the minimum void ratio

Figure 2-7 illustrates the stages of fines contents up to and beyond the FC*.

Each of the studies mentioned thus far have assumed an ideal packing scheme. That is, with increasing FC, the fines are located in the void space of the larger particles. Koltermann and Gorelick (1995) defined the concept of fractional packing to account for the fines that are not located within the voids of coarse grains, and subsequently displace the coarse particles. The fact that the coarse particles are displaced prevents the mixture from achieving the minimum porosity, or void ratio, that the ideal packing scheme would suggest (Gorelick and Koltermann 1995). For the scenario where the volume fraction of the finer material is less than the porosity, the porosity of the mixture is defined as:

$$\phi_{mixture} = \phi_c - cy(1 - \phi_f) + (1 - y)c\phi_f \qquad c < \phi_c$$

where $\phi_{mixture}$ = porosity of the mixture using the fractional packing model, ϕ_c = porosity of the coarse fraction, ϕ_f = porosity of the fine fraction, c = volume fraction of fines relative to the total volume, and y = relative amounts of coarse and fine packing.

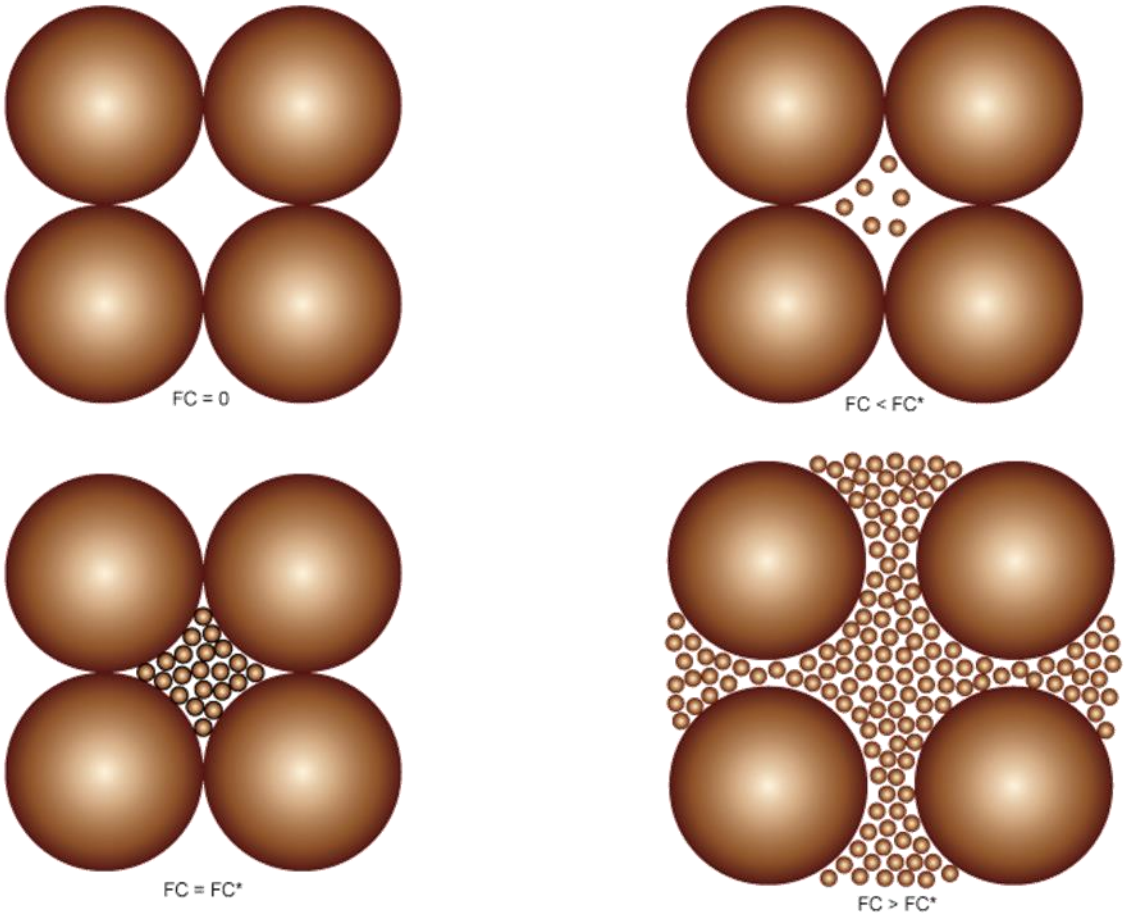

Figure 2-7 Binary mixtures are shown with varying amounts of fines contents. From left to right and top to bottom: 1. Monosized particles with 0 FC, 2. A binary mixture with FC < FC*, 3. A binary mixture at FC*, where the voids of the larger particles are completely filled with the smaller paricles. 4. A binary mixture with FC* > FC such that the larger particles are located within the matrix of smaller particles.

When the volume fraction of fines is equal to the porosity of the coarse portion, or FC*, the minimum porosity of the mixture is defined as:

$$\phi_{min} = \phi_c(1 - y_{min}) + \phi_c\phi_f \qquad c = \phi_c$$

The terms ϕ_{min} and y_{min} are the minimum porosity of the mixture and the maximum volume fraction of fines contained in the voids of the coarse particles. When the volume

fraction of fines is greater than the porosity of the coarse fraction, the porosity of the mixture is defined as:

$$\phi_{mixture} = \phi_c(1 - y) + c\phi_f \qquad c > \phi_c$$

The y and y_{min} terms are determined using experimental data from measurements of porosity, or void ratio, of mixtures.

$$y = c\left(\frac{y_{min} - 1}{\phi_c}\right) + 1 \qquad c < \phi_c$$

$$y = (c - 1)\left(\frac{1 - y_{min}}{1 - \phi_c}\right) + 1 \qquad c > \phi_c$$

$$y_{min} = 1 + \phi_f \frac{\phi_{min}}{\phi_c}$$

The value of the variable y_{min} was shown to increase with decreasing particle size ratio, d/D_{50}. For particle size ratios less than 0.01 y_{min}, varied from 0.76 to 0.80 depending on confining stress. For particle size ratios between 0.50 and 0.05, holding confining stress fixed, y_{min} varied from 0.48 to 0.85 (Gorelick and Koltermann 1995).

Kamann et al. (2007) revised the factional packing model of Gorelick and Koltermann (1995) to include five regions of porosity, rather than the three regions previously shown for the fractional packing model. The model includes regions of ideal coarse packing, disturbed coarse packing, ideal fine packing, coarse grains only and fine grains only. A new term is introduced to account for the degree to which a mixture conforms to regions one through three (Kamann et al. 2007).

Zhang et al. (2009) proposed another model for predicting porosities of binary mixtures. A mixing coefficient is introduced to account for non-ideal packing circumstances. Two regions of packing are defined and the coefficient determines the degree to which the individual constituents are mixed (Zhang et al. 2009). Lower and

upper bound porosities are determined by considering ideal packing and a zero mixing case. The zero mixing case is the mathematical combination of each individual constituent porosity, in terms of the volume fraction of the coarse and fine:

$$\phi_{mixture}{}^{UB} = b_{vc}\phi_c + b_{vf}\phi_f$$

The terms $\phi_{mixture}{}^{UB}$, b_{vc}, b_{vf} are the upper bound porosity of the mixture, the volume fraction of coarse and the volume fraction of fines, respectively. Ideal packing is defined as the lower bound porosity of the mixture.

$$\phi_{mixture}{}^{LB} = \begin{cases} \phi_c - b_{vf}(1-\phi_f), & b_{vf} < \phi_c \\ b_{vf}\phi_f, & b_{vf} \geq \phi_c \end{cases}$$

A coefficient was introduced to compute the degree of mixing:

$$\lambda = \frac{\phi^{UB} - \phi_{mixture}}{\phi^{UB} - \phi^{LB}}$$

The first two equations are substituted into the third to produce what the authors refer to as the mixing-coefficient model.

$$\phi_{mixture} = \begin{cases} (b_{vc} - \lambda b_{vc} + \lambda)\phi_c + b_{vf}\phi_f - \lambda b_{vf}, & b_{vf} < \phi_c \\ (1-\lambda)b_{vc}\phi_c + b_{vf}\phi_f, & b_{vf} \geq \phi_c \end{cases}$$

The λ term was determined by regressing measured data and data from literature to develop an average.

$$\lambda_{avg} = 0.0363\left(\frac{D_{50}}{d_s}\right) + 0.2326$$

2.5.3 Hydraulic Conductivity of Binary Mixtures

The earliest study of binary mixtures found in literature investigated the conductivity of gases through broken beds on mining sites. It was recognized that as mixtures of materials with varying particle size ratio and particle shape increased, the path the gas travelled became more tortuous. Therefore, factors were introduced to

account for increasing tortuosity related to mixtures of particle sizes, porosity of the mixtures and packing (Furnas 1929). Peck and Watson (1979) proposed an equation to predict the saturated hydraulic conductivity of mixtures of spherical particles. Bouwer and Rice (1984) proposed an equation for predicting the flow of groundwater in vadose zones composed of sand-boulder mixtures. They stated that the ratio of the saturated hydraulic conductivity of the global mixture to that of the finer material is equal to the ratio between the void ratio of the sand and the void ratio of the mixture (Bouwer and Rice 1984). This equation predicted reasonable values when compared to measured hydraulic conductivity of boulder-sand mixtures. There is also an abundance of literature on the hydraulic conductivity of sand-bentonite mixtures to investigate the hydraulic properties of landfill liners and slurry walls (Castelbaum and Shackelford 2010; Komine 2010; Sivapullaiah et al. 2000; Yeo et al. 2006).

Sand-silt binary mixtures have been investigated extensively for strength and liquefaction studies. Many of these studies include hydraulic conductivity because it affects the generation of pore pressure during undrained and partially drained loading (Bandini et al. 2009). Table 2-2 provides a summary of the studies that included saturated hydraulic conductivity of mixtures.

Table 2-2 Summary of Recent Studies of Saturated Hydraulic Conductivity of Sand Silt Mixtures

Year	Author	Reference	Material	Findings
2000	Thevanayagam	Conference Proceedings: 2nd Int. Workshop on Mitigation of Seismic Effects of Transportation Structures	ASTM Graded Sand and Non-Plastic Silt	Major decrease in k_{sat} up to FC* of approximately 30%
2006	Sathes	M.S. Thesis: New Mexico State University	ASTM 20/30 and Graded with Non-Plastic Silt	k_{sat} decreased by two orders of magnitude with up to 15% silt, by mass
2009	Bandini and Sathiskumar	Journal or Geotechnical and Geoenvironmental Engineering	ASTM 20/30 and Graded with Non-Plastic Silt	k_{sat} decreased by two orders of magnitude with up to 25% silt, by mass; volume compressibility increased and coefficient of consolidation decreased with increasing silt content
2009	Zhang et al.	Report: U.S. Department of Energy	5 mm Glass Beads with Non-Plastic Silt	Predicted the minimum void ratio of the mixture and FC* using the mixing coefficient model with modified particle diameter term
2014	Belkhatir et al.	Marine Georesources and Geotechnology	medium sand and non-plastic silt	excess pore pressure increases linearly with increasing fines content and logarithmically with intergranular void ratio; k_{sat} decreased four orders of magnitude with up to 50% silt content

A model to predict the saturated hydraulic conductivity of mixtures was developed by Gorelick and Koltermann (1995). The Kozeny-Carmen equation was modified to include the porosity the mixture, utilizing the fractional packing model.

$$k_{fp} = \left(\frac{\rho g}{\mu}\right) \frac{{d_{fp}}^2 {\phi_{mixture}}^3}{180\left(1-\phi_{fp}\right)^2}$$

Where ρ = density of the fluid, μ = dynamic viscosity of the fluid, $\phi_{mixture}$, = porosity of the mixture using the fractional packing model, and d_{fp} = grain size diameter. The grain size diameter term is volume weighted based on the volume fraction of fines in the mixture. The geometric mean grain diameter is used for FC < FC*, while the harmonic mean is used for FC = FC* and FC > FC*. Using this model, hydraulic conductivity values were successfully predicted to within one order of magnitude for 90% of data from field scale pumping and slug tests (Gorelick and Koltermann 1995).

Kamann et al. (2007) used this equation and the revised fractional packing model to predict the hydraulic conductivity of six binary mixtures. The mixtures ranged from fine sand and gravel to fine and coarse sand. The conductivity values corresponded well with predicted values. Phillips (2007) used this model to successfully predict hydraulic conductivity values using this model for natural sediments collected in-situ. The sediments ranged from gravel to fine sand.

Zhang et al. (2009) used their mixing-coefficient model as well as a revised grain size diameter term to predict values of hydraulic conductivity of five mixtures of glass beads. The grain size term was updated to a power-averaging method to avoid the discontinuity of using the harmonic mean and geometric mean based on the predetermined FC*:

$$d_{mixture} = \left(b_{vc} {d_c}^p + b_{vf} {d_f}^p\right)^{\frac{1}{p}}$$

$$p = \frac{1}{1 + e^{[a(b_{vco} - b_{vc})]}} - 1$$

The terms d_c^p and d_f^p are the representative grain size diameters of the coarse and fine fractions. The p term is an empirical coefficient that varies from 0 to -1. The term b_{vco} is the critical volume of coarse grains where the hydraulic conductivity is expected to increase abruptly. The equivalent volume fraction critical fines content would be $1 - b_{vco}$. The term a controls the steepness of the sigmoidal coefficient p. A value of 20 was found to produce reasonable predictions for measured and referenced hydraulic conductivity (Zhang et al. 2009).

2.5.4 Sample Preparation of Sand/Silt Binary Mixtures

Segregation is of significant concern during the preparation of samples of binary mixtures, and several methods of specimen preparation have been studied by past researchers. The slurry deposition method was first introduced by Kuerbis and Vaid (1988) and since has been modified by Carraro et al. (2003). For this method, the dry mass is placed into a cylinder approximately twice the volume of the specimen, and the cylinder is then filled with deaired water. The cylinder is inverted to mix the materials, and then placed under vacuum for sixteen hours, after which the slurry is inverted for five to fifteen minutes, depending on silt content, then placed onto the platen of the triaxial cell. The membrane and membrane stretcher are pulled up around the cylinder and the cylinder is lifted up slowly to deposit the specimen. It is recommended to tap the membrane stretcher with a rubber hammer while depositing to densify the specimen (Bandini et al. 2009).

Wood et al. (2008) prepared sand-non-plastic silt triaxial specimens using tapping funnel deposition (TFD), water sedimentation, the slurry deposition method, air pluviation and mixed dry tubing. The mixed dry tubing mimics the slurry deposition method, only dry. After testing, each specimen was cut open and sieved to determine the

uniformity of the specimen. The TFD retained more silt on the shell than the core. Air pluviation resulted in greater silt contents at the top of the specimen. Water sedimentation resulted in silt bands around the shell, but not within the core of the specimen. Slurry deposition and mixed dry tubing provided the most uniform specimens (Wood et al. 2008). However, an apparatus was made to invert the cylinder used for the deposition methods while directly in contact with the platen of the triaxial cell.

Ladd (1978) proposed a method to produce specimens of uniform density by under-compaction. The material is deposited in lifts. Bottom lifts have lower target densities then the upper lifts in order to not over compact the bottom portion of the specimen. Yang et al. (2006) used this method to prepare 56 triaxial specimens and reported no significant segregation. Frost and Park (2003) evaluated this method using X-ray and optical images of specimens. They found that wet pluviated and air pluviated specimens had a more uniform density.

Chapter 3

MATERIALS AND METHODS

This work was performed in two parts: in the first part, field hydraulic conductivity tests using the double ring infiltrometer were performed in the Piedmont region of Georgia. These tests were performed in order to measure infiltration rates in areas being considered for application of infiltration trenches as a stormwater BMP. In second phase of the work, lab based hydraulic conductivity tests were performed to quantify the impact of critical fines content on the conductivity of water through binary mixtures.

3.1 Infiltration Testing

The first portion of this experimental investigation measured infiltration rates in-situ to compare with published and predicted values for the Piedmont region of Georgia.

3.1.1 Materials – Infiltration Testing

The two sites were chosen for testing, and both were located in the metro Atlanta area. The first site was located in Covington, GA, and the second site was located in Lawrenceville, GA. Samples were taken from each site, for classification and index testing (Table 3-1). The rows are titled by acronyms for the site and test pit number; i.e. TPC1 is test pit Covington #1.

Table 3-1 Material from test Pits from In-Situ Testing Sites

Test Pit	Depth (m)	Soil Type	
		USDA	USCS
TPC1	0.6	sandy loam – loamy sand	SM
TPC2	0.15	sandy clay loam	CH
TPC3	0.3	loam	MH
TPL1	1	Sandy Clay Loam	CL
TPL2	1	Sandy Clay	CH
TPL3	1	Sandy Clay Loam	SC
TPL4	1	Sandy Clay	CH

Grain size distributions were determined for samples from each test pit according to ASTM D422 (Figure 3-1). The samples were taken from the bottom of the excavated pits. The soils tested ranged from sandy soils to silts to clays.

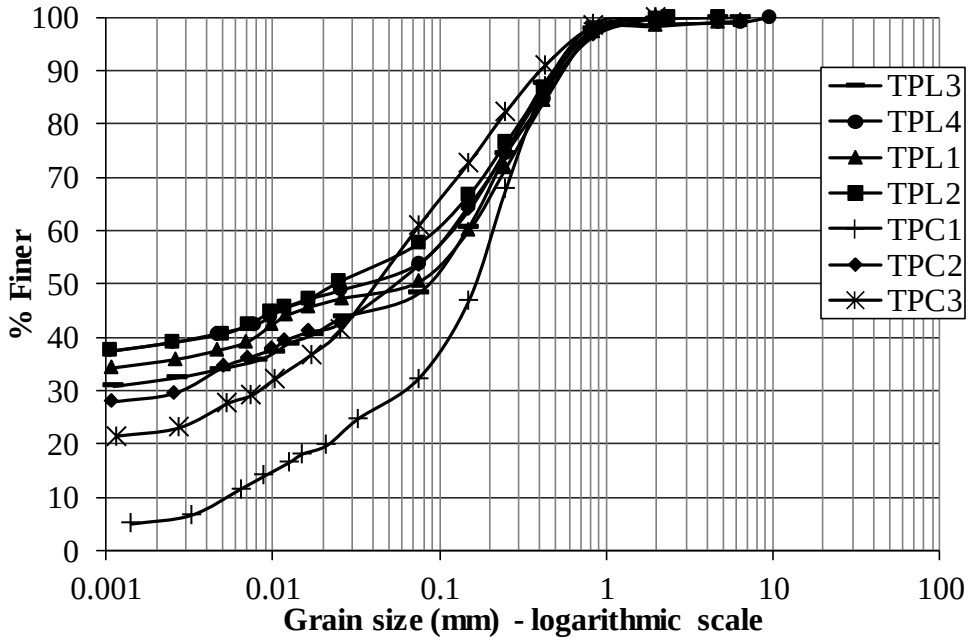

Figure 3-1 Grain size distributions are shown for the materials recovered from test pits during site work.

3.1.2 Methods – Infiltration Testing

Infiltration tests were performed according to ASTM D3385, which recommends double-ring infiltrometer (DRI) ring sizes of 12 inch (30.5 cm) and 24 inch (61.0 cm) for the inside and outside rings, with an embedment depth of between two to four inches (5.1 – 10.2 cm) to prevent sidewall leakage. For this study, the 30/60 configuration was selected. An IN14-W Heavy Duty infiltrometer was purchased from Turf Tec International. This model is composed of 14 gauge galvanized steel.

The first site work was performed in Covington, GA. The lot was provided by Georgia Department of Transportation and was located at an intersection, where the right-of-way had been extended to include a site with relatively undisturbed pine forest for a future project. Georgia 811 was contacted and the utilities were marked on the site before any work commenced.

Pits were excavated to avoid testing the hydraulic conductivity of top soil or fill and to avoid macropores created by root systems and other biological activity. The pits were excavated by manually using a shovel and pick axe. After the pits were excavated and leveled, the DRI was placed on the ground, a steel driving plate was placed on top, a 2x12 (5.1 x 30.5 cm) piece of yellow pine was placed on top of the driving plate, and a 12 pound (5.4 kg) sledge hammer was used to drive the infiltrometer into the ground. An average embedment depth of 6 cm was achieved. Lines were then connected to mariotte tubes that regulated the head in the infiltrometer. The mariotte tubes were then driven into the ground beside the DRI so that the head within the inner and annular rings would be within 5 mm. The mariotte tubes were then filled with tap water. A 15 cm soil thermometer was then installed outside the infiltrometer to monitor ground temperatures for the duration of the test. Water was siphoned from a barrel to initially fill the DRI up

to the desired level. The Mariotte tubes were then opened. Time was started as soon as the water level stabilized within the DRI. Readings were taken every fifteen minutes for the first four readings. Time increments for the remainder of the test were based on the rates recorded. More frequent readings were made for higher rates. Each test was run for a minimum of six hours (Figure 3-2).

The first three trials had to be terminated within the first one to three hours due to sidewall leakage. This was alleviated by placing bentonite around the perimeter of the DRI and tamping into place to minimize leakage.

Figure 3-2 Test set up for in-situ measurement of saturated hydraulic conductivity using a double-ring infiltrometer.

Access to the Lawrenceville, GA site was provided by Bowen & Watson Inc. An excavator was available on this site and was used to excavate four test pits. There was a layer of gravelly sand fill approximately 60 cm deep at each test pit. Hence, the pits were

excavated to approximately one meter. The excavator was also used to drive the infiltrometers. Initial water content samples were taken before testing began. All procedures were identical to the test methods followed at the Covington site, and were followed after installation of the infiltrometer. Final water contents were taken after test termination (Figure 3-3). For the Lawrenceville site, the excavation, manual clearing of cuttings and leveling of the pits, and the installation of the DRIs was accomplished in one day. All four infiltration tests were completed the next day. The disturbance due to driving the infiltrometers was considerably reduced at this site by using the excavator for insertion of the infiltrometer, compared to the previous site, which required between one and two hours to drive the DRIs with a sledge hammer, balanced with intervals of wetting the soil.

Figure 3-3 Two test pits located at the Lawrenceville, GA site are shown. A test set up is also shown in one of the test pits

For this test location, some changes were made to the operation of the Mariotte tubes. Stainless steel sleeves to hold the tubes in place during testing were fabricated, and

a wing nut was welded to the sleeve to allow the height of the Mariotte tube to be adjusted, rather than driving the Mariotte tube into the ground. An auger bit was advanced into the soil for up to seven cm. The sleeve was then driven the remaining distance using a rubber mallet. This configuration provided a more automated method for adjusting the heads in the infiltrometers at the beginning of the test.

Soil samples from each pit were collected for index testing. The Atterberg limits, grain size distribution, and water contents were measured for each test pit at each of the two sites. The liquid limit was determined using methods described in BS 1377. A correlation by Feng (2004) was used to calculate the plastic limit.

3.2 Hydraulic Conductivity of Binary Mixtures

The second portion of this experimental investigation measured the saturated hydraulic conductivity of a binary mixture of fine sand and non-plastic silt. Tests were performed using ASTM 100/200 sand as the host material, and Sil-Co-Sil 40 as the added non-plastic silt.

3.2.1 Materials – Binary Mixtures

Both materials were donated by U.S. Silica: the 100/200 sand was manually sieved from F75 sand, while the non-plastic silt, Sil-Co-Sil 40, was used as received. The 100/200 sand had a median grain diameter of 0.12 mm, while the silt had a median grain size diameter of 0.011 mm. The material properties of both base materials and that of the mixtures are given in Table 3-2. Chemical analysis was provided by U.S. Silica (Table 3-3), and the minimum and maximum void ratios were measured using methods described in ASTM D4253 and ASTM D4254. Methods 1A and C were used, respectively. A modified mold had to be used due to scarcity of the ASTM 100/200 sand. The height to diameter ratio was adhered to as closely as possible. The volume of the

modified apparatus was 203.3 cm^3. The mass of the surcharge was 13.8 ± 0.1 kPa. An anti-static cloth was required to prevent the silt from separating from the sand between minimum void ratio trials (Fuggle 2011). The grain size distribution was measured for both the base materials and mixtures according to ASTM D422 (Figure 3-4).

Table 3-2 Material Properties of Base Materials and Mixtures

Material	D_{50}	C_u	C_c	e_{max}	e_{min}
ASTM 100/200	0.120	1.63	0.78	0.860	0.566
FC 1%	0.120	1.63	0.78	0.850	0.554
FC 5%	0.120	1.63	0.78	0.836	0.549
FC 10%	0.100	4.33	2.08	0.806	0.544
FC 17%	0.095	8.67	4.15	0.835	0.51
Sil-Co-Sil 40	0.010	8.00	0.78	1.810	0.64

Table 3-3 Chemical Analysis of the Base Materials

Chemical Analysis (%)		
Material	ASTM 100/200	Sil-Co-Sil 40
SiO_2 (Silicon Dioxide)	99.8	99.7
Fe_2O_3 (Iron Oxide)	0.020	0.021
Al_2O_3 (Aluminum Oxide)	0.060	0.120
TiO_2 (Titanium Dioxide)	0.010	0.009
CaO (Calcium Oxide)	< 0.01	0.009
MgO (Magnesium Oxide)	< 0.01	< 0.01
Na_2O (Sodium Oxide)	< 0.01	< 0.01
K_2O (Potassium Oxide)	< 0.01	< 0.01
LOI (Loss On Ignition)	0.01	0.1

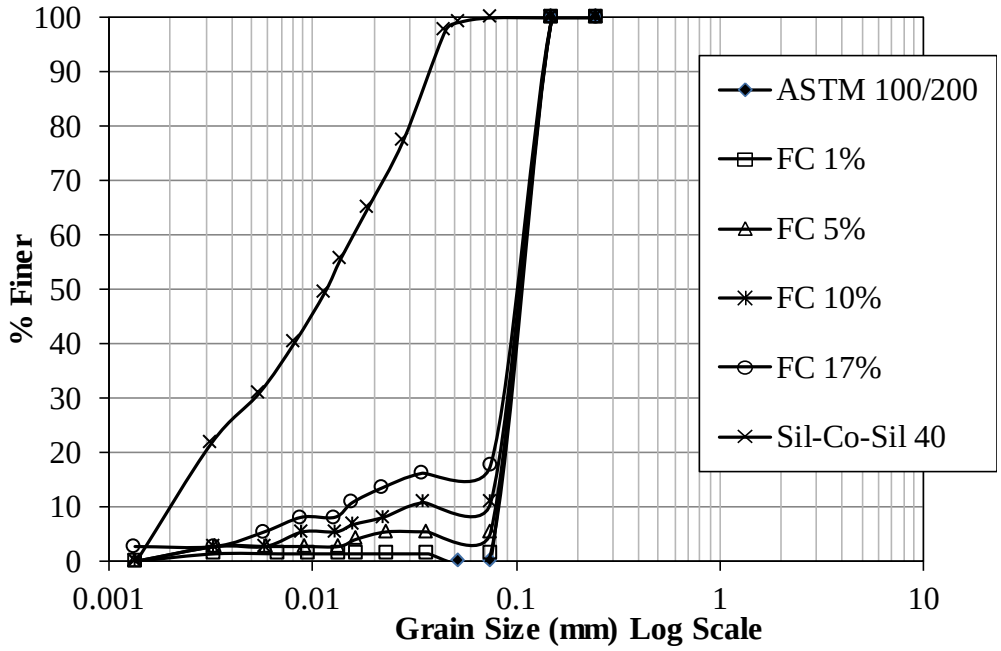

Figure 3-4 The grain size distribution is shown for the both the base materials and the mixtures.

The particle size ratio determines the mixing conditions of a binary mixture. Assuming ideal packing, if $d_s > 0.414D_{50}$, the fine particles cannot be retained in the pore space of the coarse particle at any packing condition. If $0.414D_{50} > d_s > 0.155D_{50}$ the fine particles can be retained in the pore space of the coarse particles only when the coarse particles are in a loose packing condition when the fines content is relatively low. For the scenario where $d_s < 0.155$, the fine particles will be retained in the pores of the coarse particles at any packing conditions of the coarse particles up to the upper bound FC* estimation (Choo and Burns 2014).

Tests were performed with fines contents of 1, 5, 10, 17, and 100%, and at relative densities of 20% and 70% (Table 3-4).The percentage of fines content in each mixture were chosen by estimating the critical fines content (FC*) using methods described in Choo and Burns (2014). Incremental values were chosen up to the critical fines content of 17% by mass. Table 3-5 shows the range of possible FC*. Fines contents

beyond the lower bound estimate of 17% were not considered to ensure $d_s < 0.155D_{50}$, so that the silt grains could theoretically be retained in the pore space of the sand with either loose or dense packing conditions.

Table 3-4 Experimental Matrix of Binary Mixtures for Hydraulic Conductivity Testing

Type	Host Material	Added Material	
	ASTM 100/200	Sil-Co-Sil 40	Sil-Co-Sil 40
D_{50}	0.12	0.011	0.011
Size Ratio	-	0.09	0.09
Initial Density	20 - 70%	20%	70%
Fines Content	-	1	1
	-	5	5
	-	10	10
	-	17	17
	-	100	100

Table 3-5 Calculated Critical Fines, FC*, for the Sand-Silt Mixture

ASTM 100/200	Sil-Co-Sil 40	
	e_{max}	e_{min}
e_{max}	0.234	0.344
e_{min}	0.168	0.257

3.2.2 Methods – Binary Mixtures

Saturated hydraulic conductivity tests were performed using a flexible wall permeameter according to ASTM D5084. The tests were performed in a triaxial cell, using a pressure panel for pressure controls (Trautwein Soil Testing Equipment). GEOTAC (Geotechnical Test Acquisition and Control) pressure transducers and

corresponding software were used to monitor cell and pore pressures and to obtain B-values for saturation.

Several of methods of sample preparation were investigated in this study. The slurry deposition method was first explored. While the method has worked for sand mixtures, segregation was observed when using the ASTM 100/200 sand / non-plastic silt mixture. After the final inversions to mix the specimen, approximately five minutes were required to roll the membrane up the cylinder, install the membrane stretcher, and apply vacuum. During these five minutes, a significant amount of silt segregated and formed a slurry above the sand. This slurry had to be siphoned off, taking with it the majority of the silt. Also, when tapping the apparatus to densify the slurry, a significant amount of silt migrated to the top of the specimen. Water pluviation resulted in significant silt banding at every lift. Moist tamping resulted in the same segregation problem as the slurry deposition method densification. The method that consistently produced homogenous specimens was dry tubing. By using a funnel with an enlarged opening and allowing as little falling distance as possible, the specimen appeared homogenous relative to the previous methods. To densify the specimen, the stretcher was tapped in a circular pattern while depositing, still with as little falling distance as possible. Specimens with relative densities of approximately 20 and 70% were consistently achieved. This method worked well for each FC in terms of producing uniform specimens, but acceptable B-values were not achieved for 10 and 17% silt contents after several trials.

To prepare the 10, 17 and 100% FC specimens, the same method of deposition was employed, but in seven lifts. After each lift deaired water was slowly added with a laboratory wash bottle. Water was slowly added to each lift until the top of the lift was

just saturated. No segregation or silt banding was observed for the 20% relative density specimens produced using this method. Some segregation was observed for the densified specimens, but considerably less so than for the previously attempted methods.

After the specimen was formed, filter paper, a saturated porous stone and top platen were placed on top. The lines were connected and a vacuum of approximately 34 kPa was applied to the top while measurements were taken of the specimen, and the cell was assembled and filled. After the cell was filled, a small confining pressure of 14 to 28 kPa was gradually applied and the vacuum was removed. To initially soak the specimens prepared using the dry deposition, deaired water was allowed to gravity feed through the bottom of the specimen. Care was taken to use relatively small heads so that the silt would not be washed form the pore space of the sand. This continued until there was no visible air evacuating from the specimen. A back pressure of 35 kPa was then applied. Back pressuring overnight was sufficient for specimens of sand and 1% silt content. For 5% silt specimens were flushed while under backpressure for up to two days. B-values of at least 0.95 were achieved for all specimens.

The wet prepared specimens were also initially soaked by flushed deaired water through the bottom of the specimen. There was little air observed evacuating from the specimens relative to the specimens prepared using the dry method. The wet prepared specimens were back pressured overnight and achieved B-values of at least 0.95.

All specimens were tested using the falling head – rising tailwater methods described ASTM D5084. Four points were recorded at a confining pressure of 35 kPa using similar head differences to ensure repeatability. After which the specimen was consolidated by an additional 35 kPa. This process was repeated four times for each

specimen up to 140 kPa to observe the effect of confining stress on saturated hydraulic conductivity. Care was taken not to use excessive hydraulic gradients. The highest head differences employed were 3.4 and 6.2 kPa for the17% and 100% silt specimens, respectively. Specimens were oven dried overnight at 160^{o} C to measure the final water content. Wet sieving was then employed to verify the fines content.

3.2.3 Material Selection

Several mixtures were considered before selecting the tested sand-silt mixtures. ASTM 20/30, ASTM 60/80, ASTM Graded sand and ASTM 100/200 were all considered. According to ASTM D5084, the flexible wall method should be used with materials with saturated hydraulic conductivities lower than 1 x 10^{-4} cm/s. Hence, several trails of hydraulic conductivity tests, all using the falling head-rising tailwater methods previously covered, were run on each of these proposed materials.

The flow rates of the systems with and without porous stones and filter paper were determined on two pressure panels and triaxial cells. Four types of porous stones were used on two different pressure panels to calibrate each system. The porous stones were selected based on ranging porosities. Each porous stone was saturated under approximately 68 kPa of vacuum overnight. Measured flow rates for porous stones with and without filter paper were indistinguishable, therefore only measured flow rates for porous stones with filter paper are shown in Table 3-6

Table 3-6 Measured Flowrates Using Porous Stones of Varying Porosities and of the System Without Porous Stones

Material	Flowrate (cm^3/s)
Blue P.S. w/ Filter Paper	0.110
Yellow P.S. w/ Filter Paper	0.180
Black P.S. w/ Filter Paper	0.095
Glass Fritted Disc (Extra Coarse) w/ Filter Paper	0.110
System w/o P.S. - Station C	0.170
System w/o P.S. - Station B	0.210

Figure 3-5 shows the measured flow rates from the various materials plotted with the system they were measured with. All tests were run using hydraulic gradients similar to those expected to be used for the testing regime. ASTM 20/30, Graded, 60/80 and 100/200 were all prepared using dry funnel deposition. Similar target densities were used. B-values of at least 0.95 were achieved for each test. Measured flow rates, or hydraulic conductivity, of the ASTM 20/30, Graded and 60/80 were found to be indistinguishable from the test apparatus. After four trials, the ASTM 100/200 sand was consistently two to three times lower than the measured flow rate of the system. Also, consistent changes in hydraulic conductivity with specimen density and confining stress were observed for the 100/200. For the ASTM 20/30 and 60/80, no distinguishable changes were observed with increasing density or confining stress. Consequently, the ASTM 100/200 sand and Sil-

Co-Sil 40 mixture was selected to ensure the hydraulic conductivity of the system was greater than the material being tested.

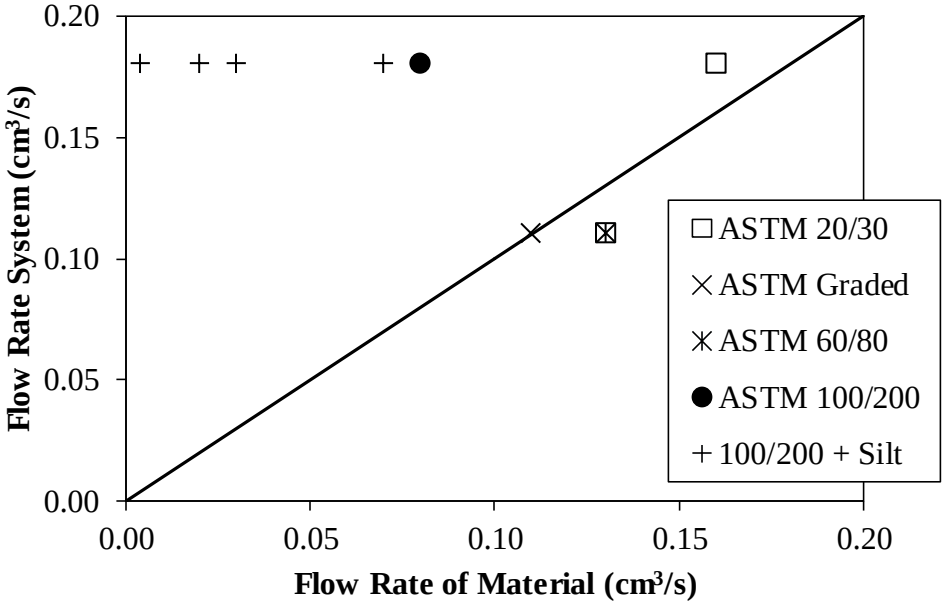

Figure 3-5 Measured flow rates of varying sands are shown vs. the measured flow rates of the flexible wall hydraulic conductivity system. The ASTM 20/30, Graded, and 60/80 sands are indistinguishable from the measured flow rates of the apparatuses.

Chapter 4

RESULTS and ANALYSIS

4.1 Infiltration Measurements and Predictions

Results of the double ring infiltrometer Infiltration tests performed on the Piedmont soil in Covington GA are given in Figure 4-1. Data are shown for Test Pit 2 and Test Pit 3 only, as the data gathered for Test Pit 1 were considered unreliable. The measured rates for TPC2 and TPC3 were relatively constant over the entire measuring interval, and were attributable to the wetting of the surface during test setup to aid in driving the infiltrometers. Consequently, the resulting measurements represent saturated hydraulic conductivity, with relatively little impact of capillarity during the initial operation of the test. The infiltration rates in these soils reached a steady state value of between $1 – 2 \times 10^{-4}$ cm/sec, which is consistent with previous measurements in similar soils (Estes 2007; Stewart 1964).

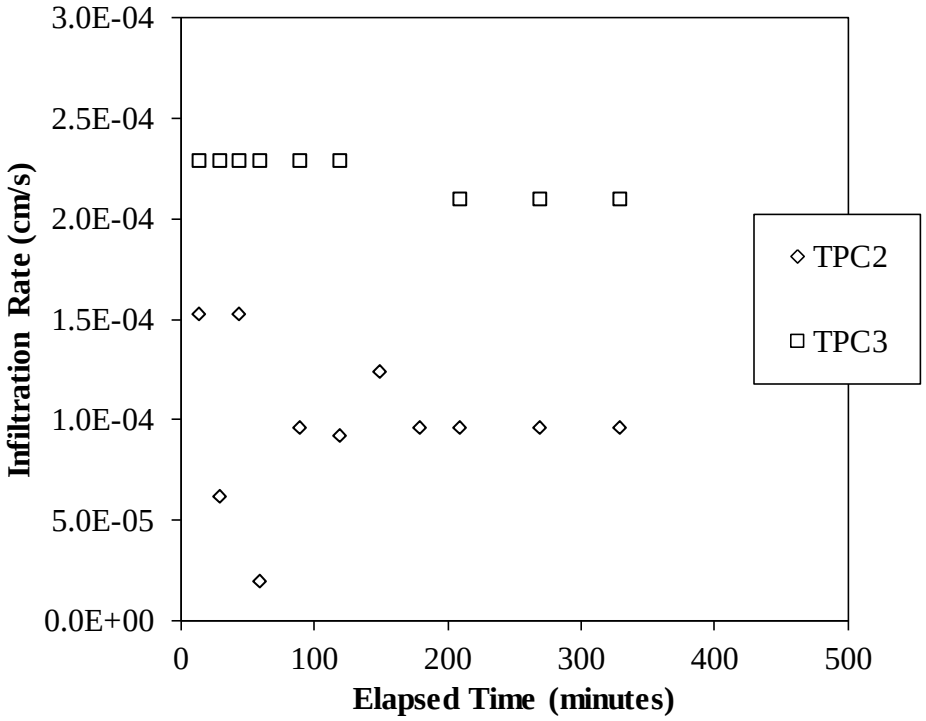

Figure 4-1 In-situ infiltration rates were measured using a double-ring infiltrometer. The site was located in Convington, GA in the Piedmont physiographic region

Infiltration rates measured for the four test pits at the Lawrenceville site demonstrated the clear influence of capillarity, with infiltration rates decreasing as elapsed time progressed (Figure 4-2). Steady state infiltration rates measured at the Lawrenceville site ranged over an order of magnitude, from a low of 1×10^{-5} cm/sec to a high of 3×10^{-4} cm/sec. Test Pits 1, 3, and 4 had infiltration rates that varied within the range of 1×10^{-5} cm/sec to roughly 8×10^{-5} cm/sec. This level of variability in hydraulic parameters is not uncommon in soils of saprolitic origin.

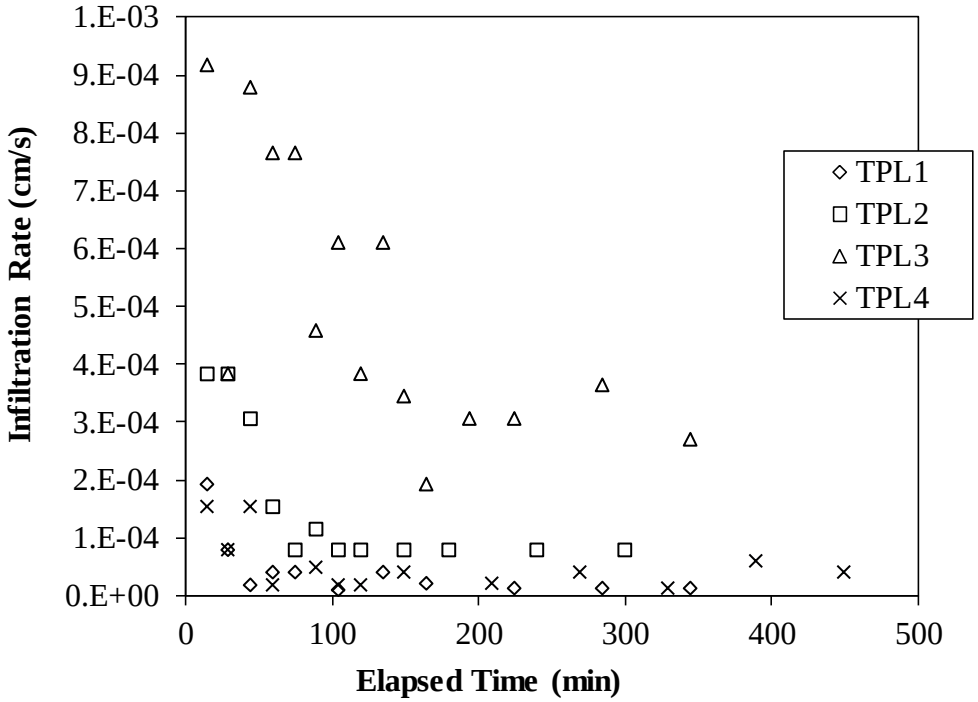

Figure 4-2 In-situ infiltration rates were measured using a double-ring infiltrometer. The site was located in Lawrenceville, GA in the Piedmont physiographic region.

The saturated hydraulic conductivity measured during a double ring infiltrometer test is typically taken to be the final, or steady-state, rate of infiltration. A comparison of the experimentally measured values with database and predicted values are given in Table 4-1. The NRCS values are taken from the database maintained by the National Resources Conservation Service, while the ROSETTA values were predicted using the sand, silt and clay contents of the soils as inputs to the US Department of Agriculture's ROSETTA model. Comparison of the in situ measured values with the NRCS database and the values predicted using the ROSETTA model show that the NRCS figures over predict the field measured values (Figure 4-3). However, the ROSETTA model, using the soil grain size distribution curve as input, gave values that were more closely aligned with the field measured values (Figure 4-4).

Table 4-1 Measured and Predicted Values of Hydraulic Conductivity

Test Pit	Saturated Hydraulic Conductivity, k_{sat} (cm/s)		
	NRCS	In-Situ	ROSETTA
TPC2	2.8×10^{-3}	9.5×10^{-5}	3.3×10^{-4}
TPC3	9.0×10^{-4}	2.4×10^{-4}	7.8×10^{-5}
TPL1	9.0×10^{-4}	9.5×10^{-6}	1.2×10^{-4}
TPL2	9.0×10^{-4}	7.6×10^{-5}	1.1×10^{-4}
TPL3	9.0×10^{-4}	2.6×10^{-4}	1.2×10^{-4}
TPL4	9.0×10^{-4}	3.8×10^{-5}	1.2×10^{-4}

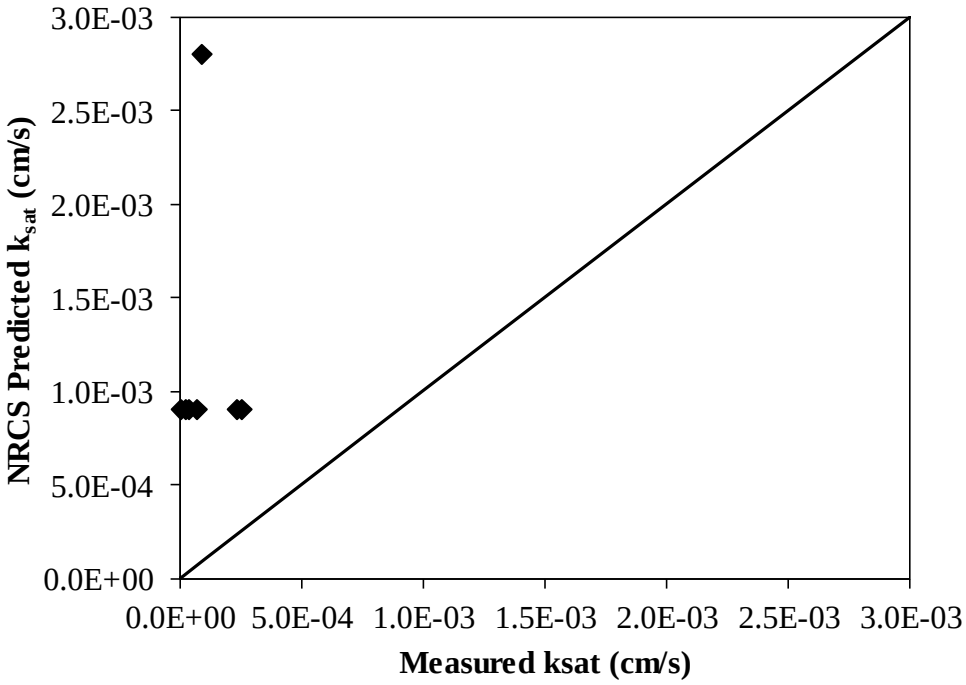

Figure 4-3 Measured values are plotted with predicted values of saturated hydraulic conductivity. The measured values are taken from double-ring infiltrometer data. The predicted values were taken from NRCS Soil Survey Data. The NRCS estimates over predicted the measured estimates in each case.

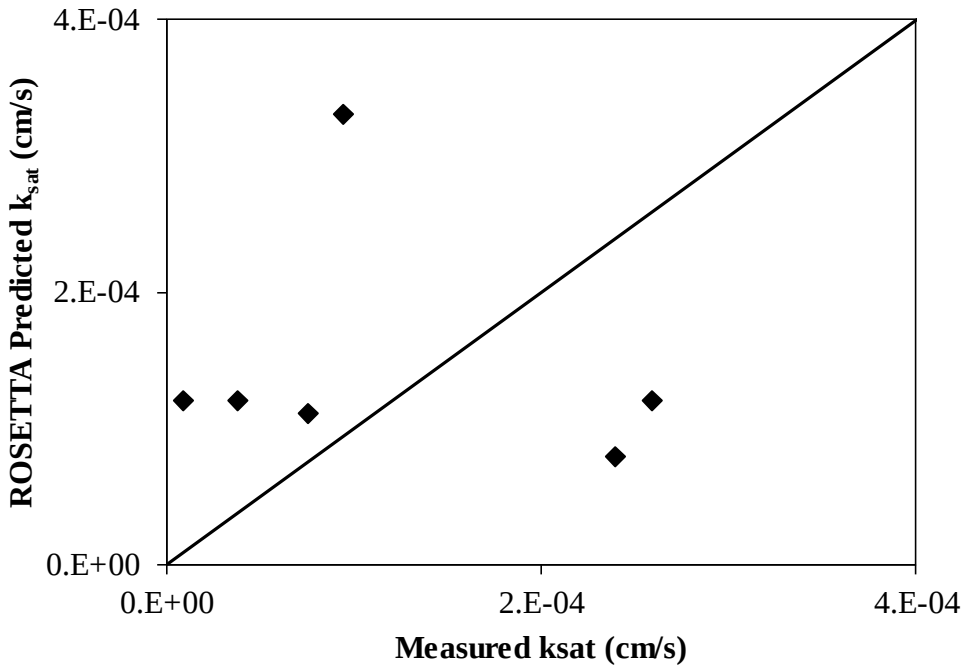

Figure 4-4 Measured values are plotted with predicted values of saturated hydraulic conductivity. The measured values are taken from double-ring infiltrometer data. The predicted values were taken from the podetransfer software ROSETTA.

4.2 Philip Parameters

In addition to the ROSETTA model, the experimental data were also fitted to the Philips Equation for infiltration. The Philips parameters were treated as empirical constants and estimated by the measured infiltrometers data using the method of least-squares (Table 4-2 and Figures 4-5, 4-6, 4-7 and 4-8). Reasonable agreement was found for the four test pits in Lawrenceville; however, the relatively sharp decrease in measured data for Test Pit 1 resulted in an unrealistically high sorptivity value.

The goal of curve fitting is to minimize the error of a physically meaningful model, not to find a model that minimizes error (Santamarina and Fratta 2005). The measured infiltrometer data from Covington was recorded under saturated conditions due

to repeated wetting in order to advance the infiltrometers, hence determining sorptivity parameters would be physically meaningless.

Table 4-2 Least-Squares Estimates of Philip Parameters

Test Pit	Philip Equation Parameters	
	S_p (cm/s$^{1/2}$)	K_p (cm/s)
TPL1	1.75×10^{-3}	9.42×10^{-6}
TPL2	2.29×10^{-3}	1.00×10^{-6}
TPL3	7.22×10^{-3}	9.01×10^{-5}
TPL4	7.75×10^{-4}	3.99×10^{-6}

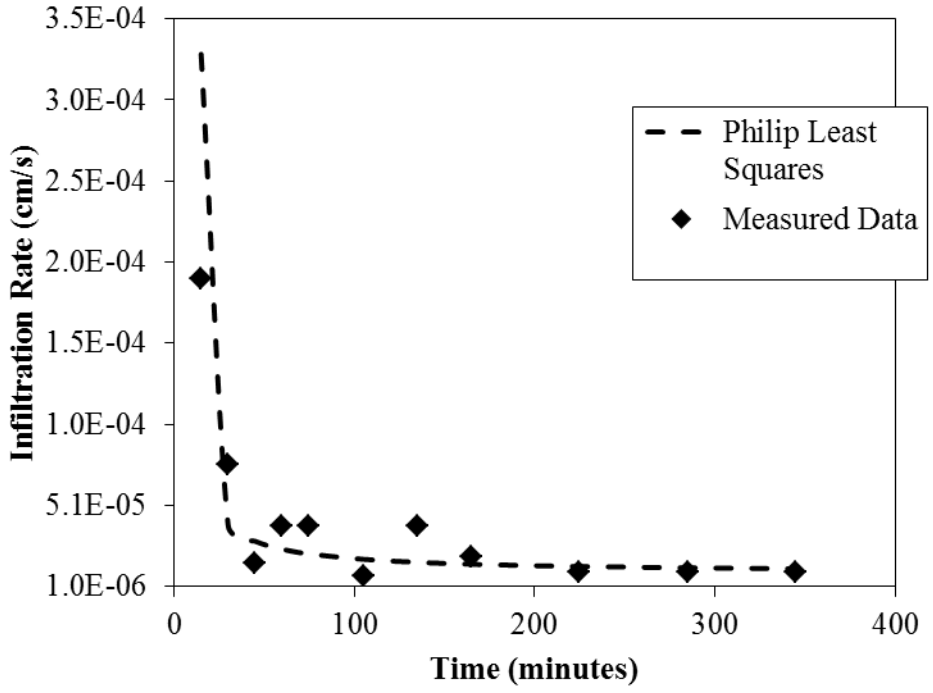

Figure 4-5 Philip parameters where estimated using least-squares with measured infiltrometer data. The data was gathered from TPL1 in Lawrenceville, GA.

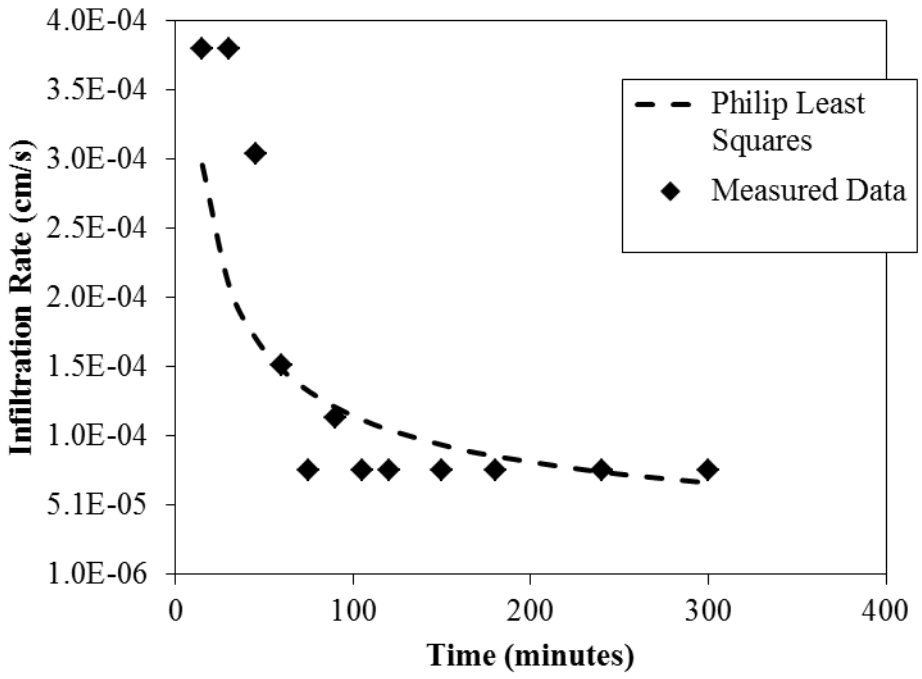

Figure 4-6 Philip parameters where estimated using least-squares with measured infiltrometer data. The data was gathered from TPL2 in Lawrenceville, GA.

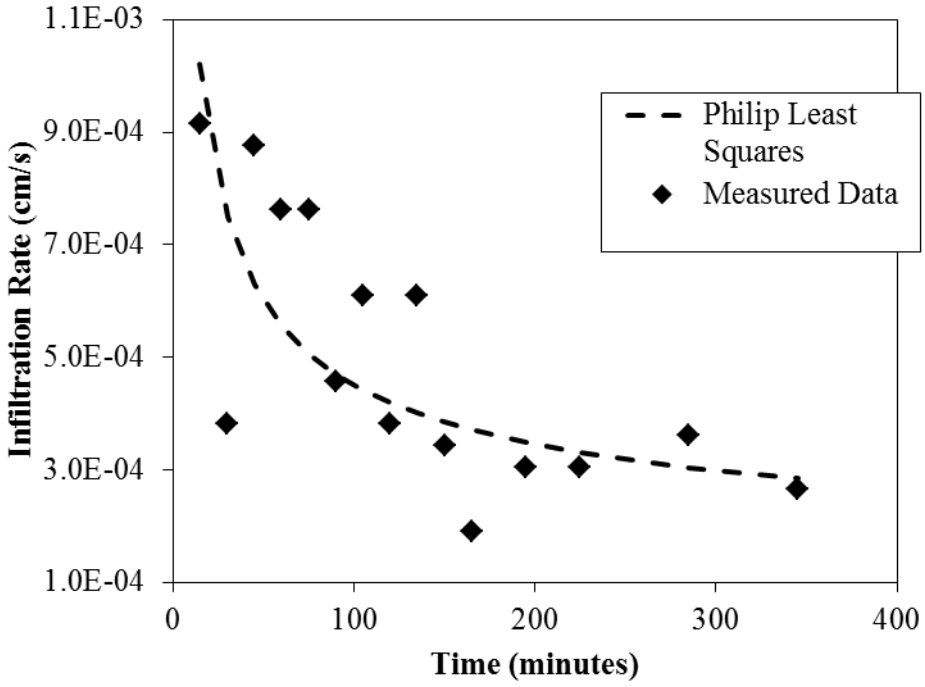

Figure 4-7 Philip parameters where estimated using least-squares with measured infiltrometer data. The data was gathered from TPL3 in Lawrenceville, GA.

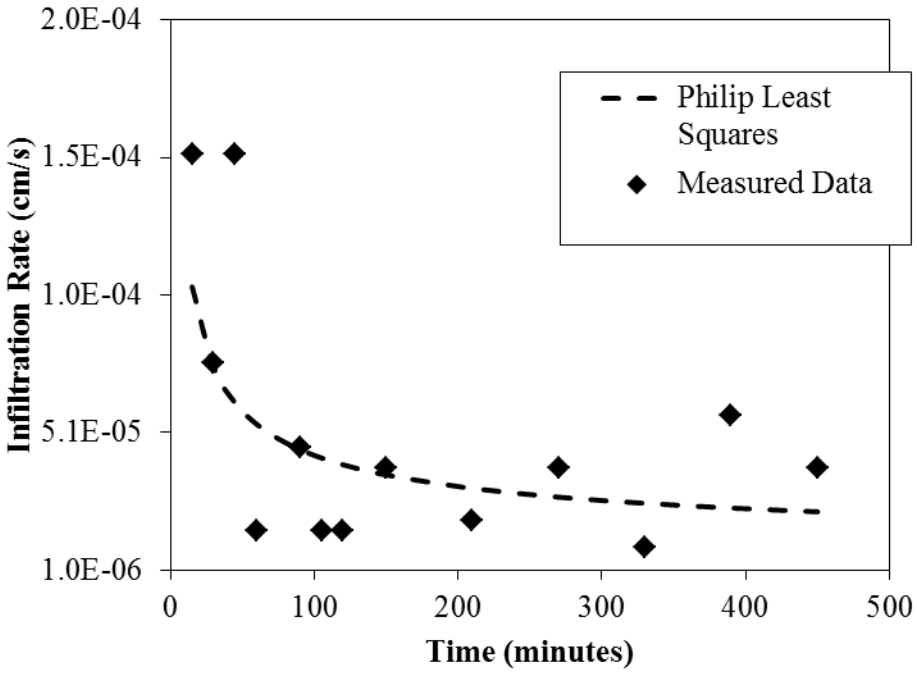

Figure 4-8 Philip parameters where estimated using least-squares with measured infiltrometer data. The data was gathered from TPL4 in Lawrenceville, GA

4.3 Extreme Void Ratios

The maximum and minimum void ratios of the mixtures were measured using methods described in ASTM D4254 and ASTM D4253. Methods C and 1A were used, respectively (Figure 4-9 and Figure 4-10). The results were evaluated using the Fractional Packing Model by Gorelick and Koltermann (1995) and the Zhang et al. (2009) model was used to predict the measured minimum and maximum void ratios (Figure 4-11 and Figure 4-12). The fractional packing model resulted in an artificial minimum which has been observed by previous studies (Kamann et al. 2007). The mixing-coefficient model consistently under predicted the void ratio of the mixture relative to the measured data (Figure 4-13 and Figure 4-14). The λ_{avg} value was used to compare results of this study with published results in subsequent sections of this chapter.

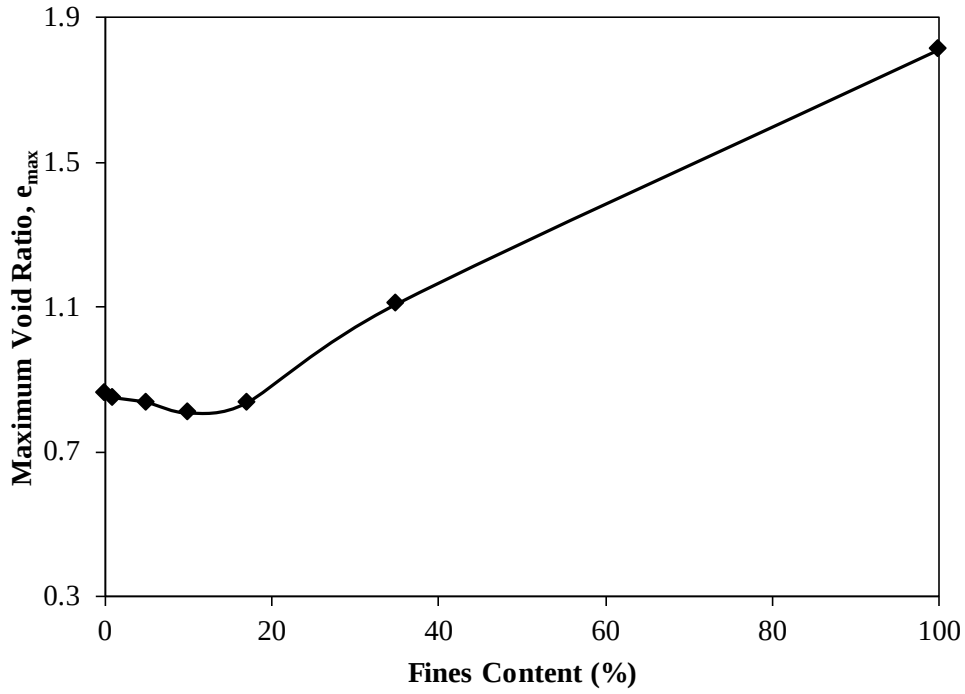

Figure 4-9 Measured maximum void ratios for ASTM 100/200 sand with increasing Sil-Co-Sil 40 content.

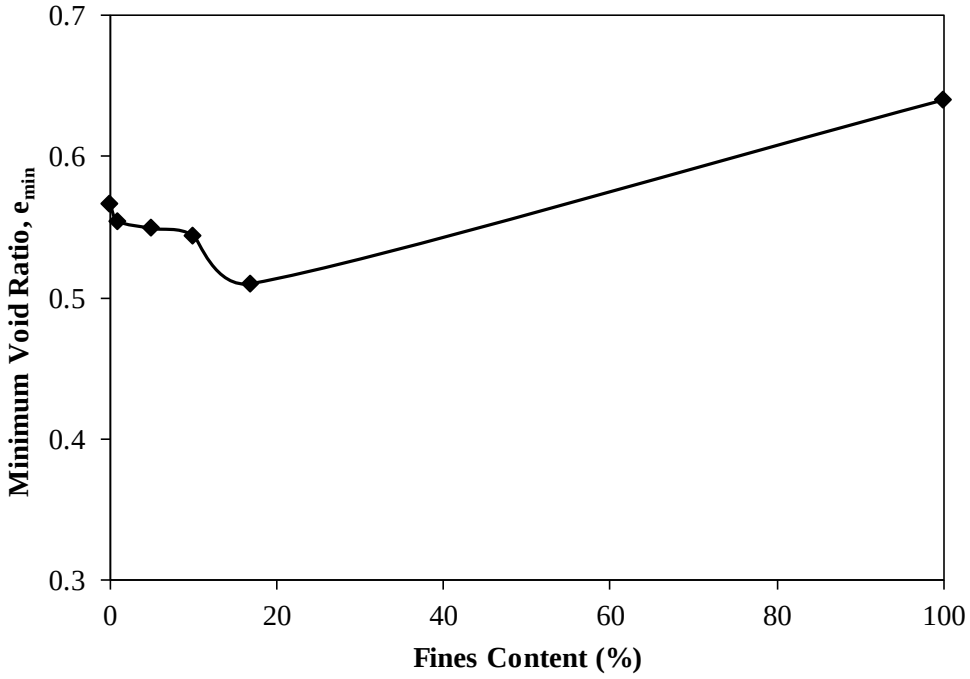

Figure 4-10 Measured minimum void ratios for ASTM 100/200 sand with increasing Sil-Co-Sil 40 content

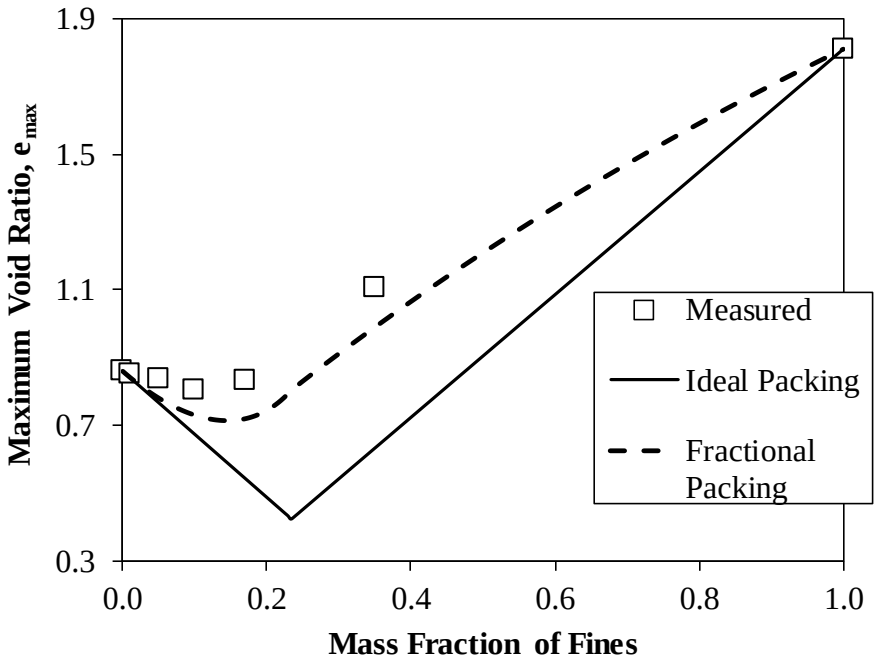

Figure 4-11 The Fractional Packing Model from Gorelick and Koltermann (1995) was used to predict the maximum void ratio of an ASTM 100/200 sand mixed with increasing Sil-Co-Sil 40 content.

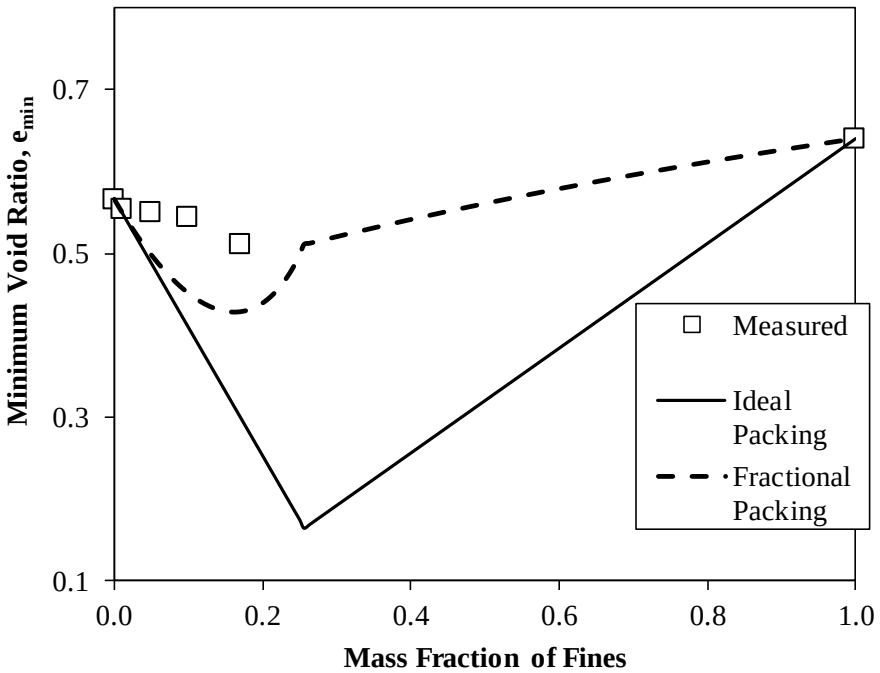

Figure 4-12 The Fractional Packing Model of Gorelick and Koltermann (1995) was used to predict the minimum void ratio of an ASTM 100/200 sand mixed with increasing Sil-Co-Sil 40 content.

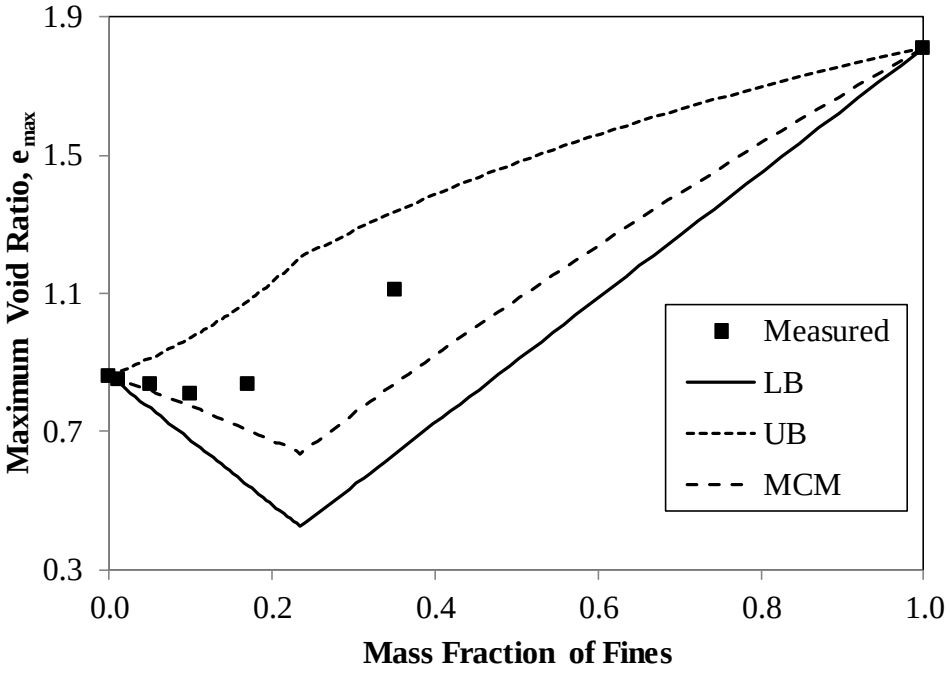

Figure 4-13 The mixing-coefficient model of Zhang et al. (2009) was used to predict the maximum void ratio of an ASTM 100/200 sand mixed with increasing Sil-Co-Sil 40 content.

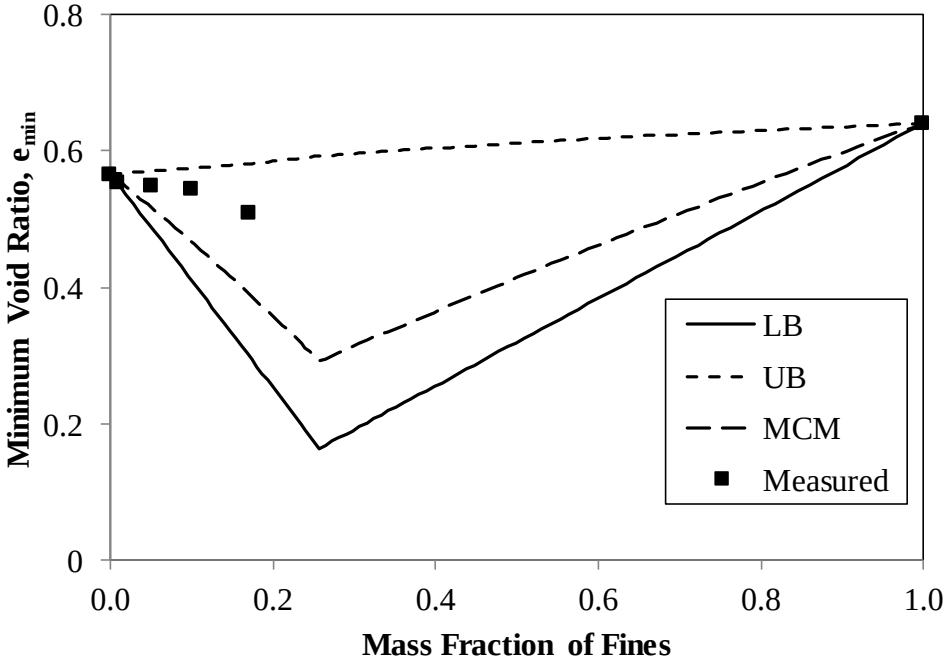

Figure 4-14 The mixing-coefficient model of Zhang et al. (2009) was used to predict the minimum void ratio of an ASTM 100/200 sand mixed with increasing Sil-Co-Sil 40 content

4.4 Silt Content and Hydraulic Conductivity

The saturated hydraulic conductivity of an ASTM 100/200 sand mixed with Sil-Co-Cil 40 non-plastic silt in a binary mixture was measured using a flexible wall permeameter. Falling head-rising tailwater methods were used as described ASTM D5084, and two target relative densities were used for the sand-silt mixtures: 20 and 70%. The measured hydraulic conductivity decreased with increasing silt content for both loose and dense specimens by two orders of magnitude (Figure 4-15and Figure 4-16). The hydraulic conductivity also decreases with increasing density. Both of these findings agree with those found in literature (Bandini et al. 2009; Belkhatir et al. 2014; Sathees 2006; Thevanayagam and Martin 2000). All values shown were measured with a confining pressure of 35 kPa. The 100% silt specimen was tested at one fixed density, ρ_d = 1.3 g/cm^3, for a reference value.

There is a greater than one order of magnitude drop between 0 and 17% silt contents for both the loosely and densely prepared specimens. After the 17% FC, the estimated FC* using the Choo and Burns (2014) model, the decrease is relatively smaller. As the fines content increased up to the FC*, the void space decreased and the surface area contributing to viscous drag increased, but the addition of fines beyond the FC* resulted in the loss of contact between the coarse particles (Figure 4-17). From this point, the saturated hydraulic conductivity, and global behavior of the soil specimen in general, exhibited behavior similar to that of the fines. Similar changes in the rate of decrease have been observed in recent literature (Belkhatir et al. 2014).

Although steps were taken to prepare homogenous specimens, segregation during specimen preparation or migration of silt during permeation is always a concern for sand-silt specimens. Relatively small segregation of silt was observed for the densely prepared

specimens. However, the loosely prepared specimens were visually homogenous. Segregation in the densely prepared specimens could have induced lower conductivity values.

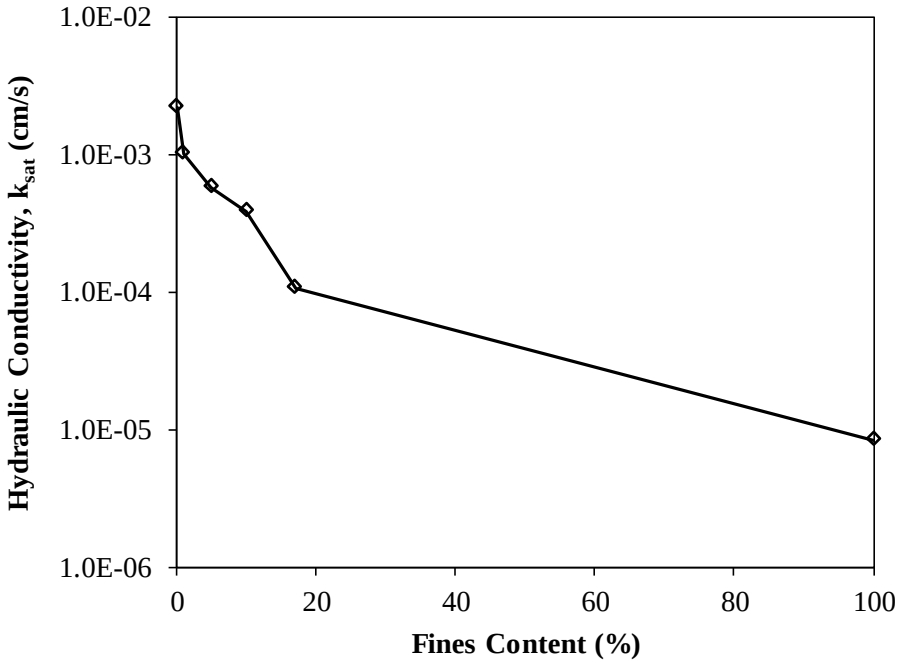

Figure 4-15 Saturated hydraulic conductivity of ASTM 100/200 sand with increasing Sil-Co-Sil 40 content. Specimens prepared relatively loose, Dr = 20%.

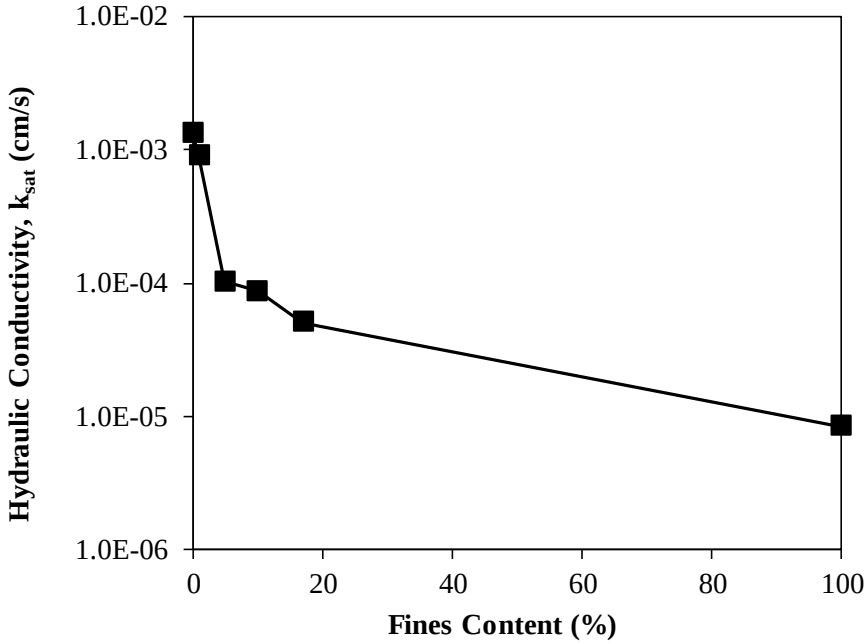

Figure 4-16 Saturated hydraulic conductivity of ASTM 100/200 sand with increasing Sil-Co-Sil 40 content. Specimens prepared relatively dense, Dr = 70%.

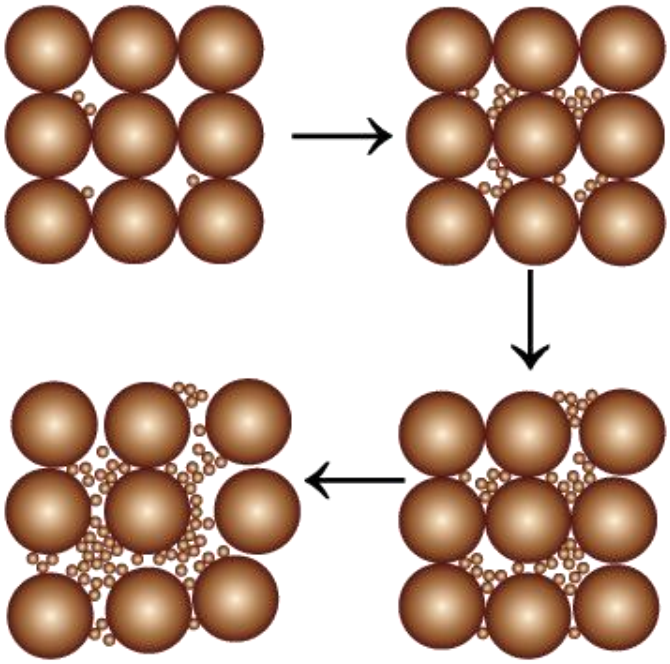

Figure 4-17 As the fines content increases the matrix of coarse particles is separated by the fine grains. At this point the global behavior of the soil is expected to behave similarly to the fine grained material.

4.5 Global Void Ratio and Intergranular Void Ratio and Saturated Hydraulic Conductivity

The global void ratio was calculated for each specimen using the known mass of solids and total volume, with target void ratios to achieve target relative densities. The measured hydraulic conductivity was analyzed as a function of both the global and intergranular void ratio (Figure 4-18 and Figure 4-19). As expected, the hydraulic conductivity decreased with decreasing global void ratio and increasing intergranular void ratio for each sand silt mixture. The trend in Figure 4-18 shows the expected decrease in hydraulic conductivity with decreasing void ratio. However, the decrease in void ratio resulted in larger decreases in hydraulic conductivity for specimens containing greater than 1% silt. The decrease in void ratio of the sand/silt mixtures may lead to a greater decrease in volume due to the presence of fines already contained in the pore volume.

Figure 4-19 shows that as silt content increases, the intergranular void ratio increases and the hydraulic conductivity decreases. This observation agrees with those found in literature (Belkhatir et al. 2014; Sathees 2006). All values shown were measured with a confining pressure of 35 kPa.

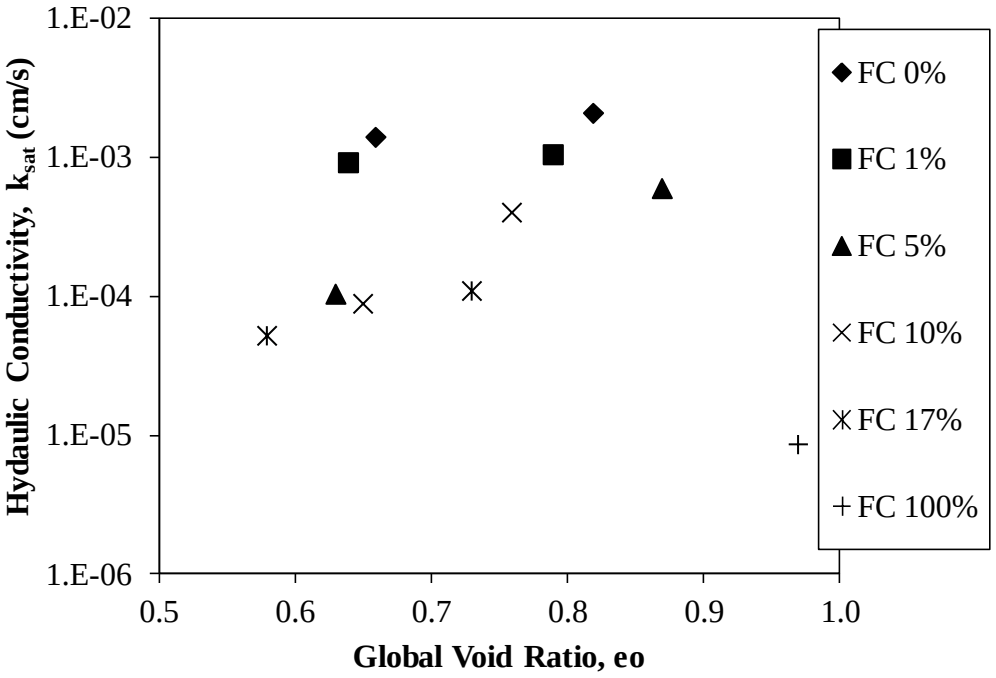

Figure 4-18 The saturated hydraulic conductivity of ASTM 100/200 sand with increasing contents of Sil-Co-Sil 40 is shown as a function of global void ratio.

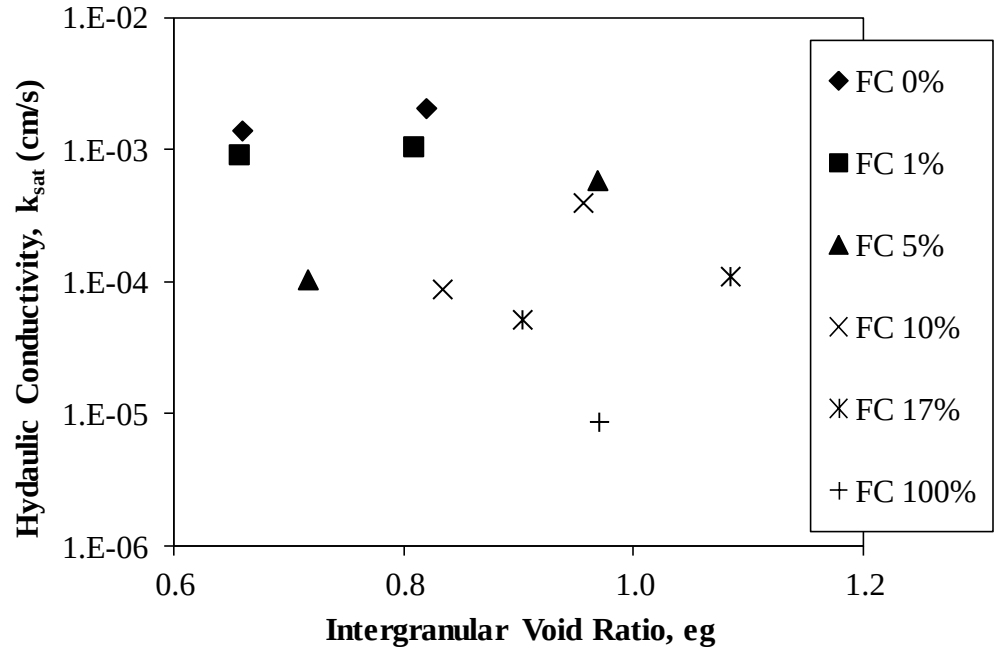

Figure 4-19 The saturated hydraulic conductivity of ASTM 100/200 sand with increasing contents of Sil-Co-Sil 40 is shown as a function of intergranular void ratio.

4.6 Confining Pressure and Hydraulic Conductivity

Each specimen was back pressured and tested with an effective stress of 35 kPa (5 psi). After measurements were taken at 35 kPa, the specimen was consolidated by an additional 35 kPa up to 140 kPa to assess the relationship between confining stress and hydraulic conductivity. Consolidation required less than five minutes for sand samples and over an hour for the 100% silt specimens. Figure 4-20 shows the hydraulic conductivity as a function of confining stress for loose specimens, and Figure 4-21 shows the values for dense specimens.

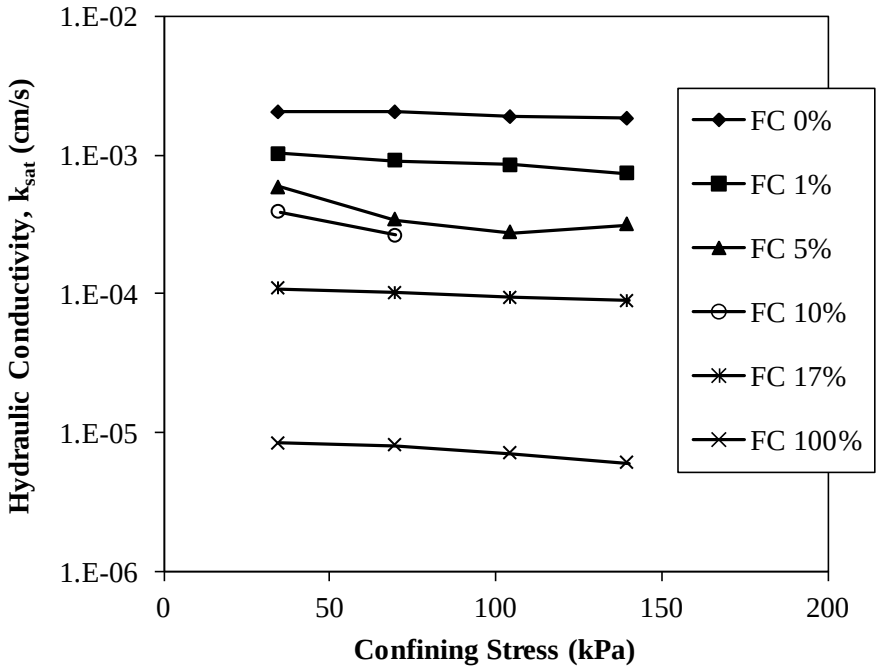

Figure 4-20 Hydraulic conductivity is shown as a function of confining stress for loosely prepared specimens of sand-silt mixtures.

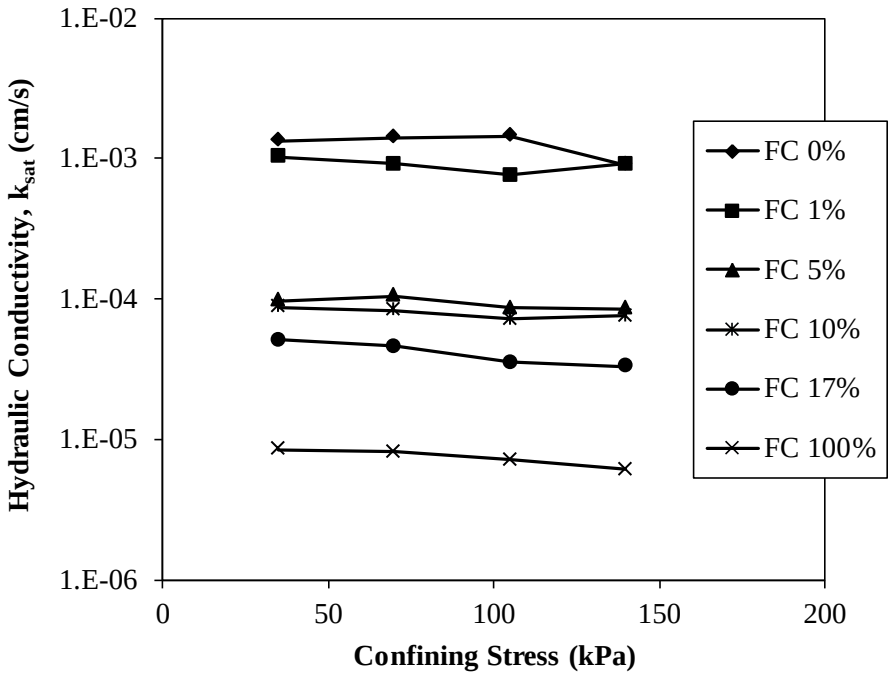

Figure 4-21 Hydraulic conductivity is shown as a function of confining stress for densely prepared specimens of sand-silt mixtures.

4.7 Predicting Hydraulic Conductivity of Binary Mixtures

The mixing coefficient model was used to predict the saturated hydraulic conductivity of the sand-silt mixture (Figure 4-22 for loose specimens and Figure 4-23 for dense specimens). The terms UB, MCM, and LB are upper bound, mixing-coefficient model and lower bound, respectively. The UB prediction was generated assuming there was no mixing. The LB uses the ideal packing model, and the MCM used the estimated λ_{avg} value. λ_{avg} was calculated according to the methods outlined in Zhang et al.(2009). The λ value can be changed based on measured void ratios to more accurately reflect the level of mixing between the sand and silt for predicting extreme porosities, or void ratios. However, the mixing-coefficient model consistently over predicted hydraulic conductivity measured for the ASTM 100/200 and Sil-Co-Sil 40 mixture.

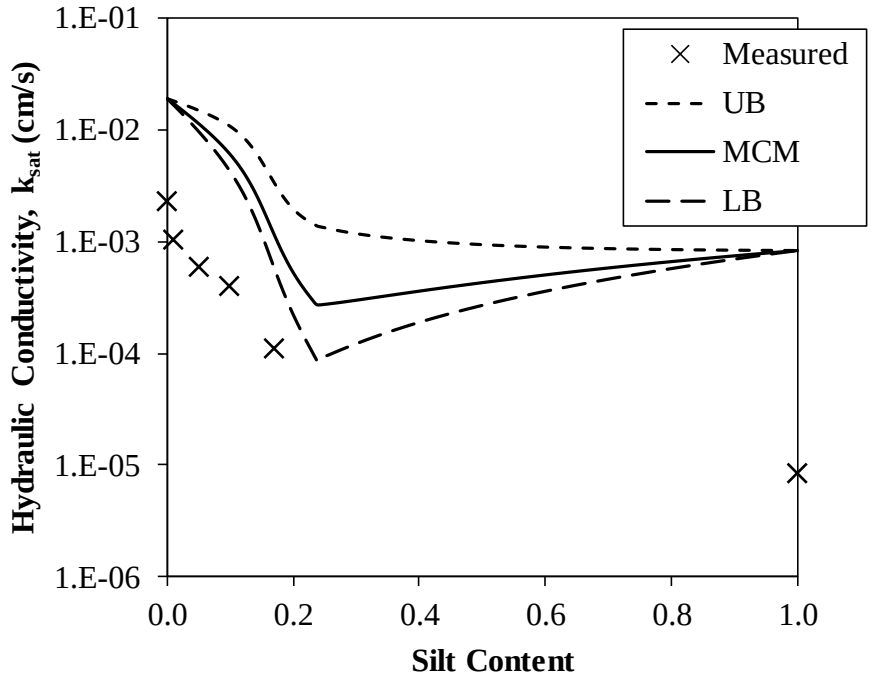

Figure 4-22 The mixing-coefficient model of Zhang et al. (2009) was used to predict the hydraulic conductivity of the loosely prepared specimens.

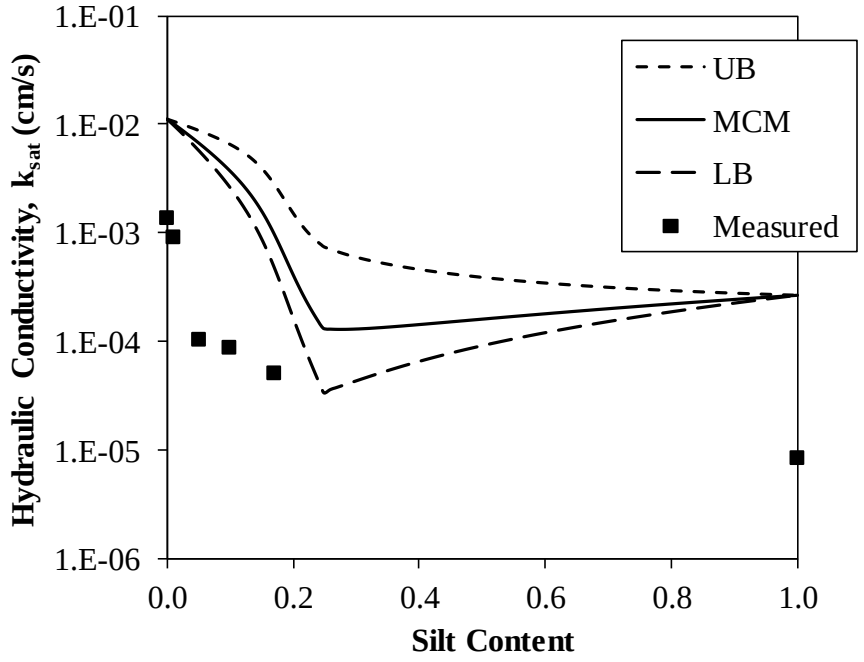

Figure 4-23 The mixing-coefficient model of Zhang et al. (2009) was used to predict the hydraulic conductivity of the densely prepared specimens.

4.8 Discussion – Infiltration

For the infiltration tests at the Lawrenceville site, there were variations between rates in early readings, particularly with TPL1. These variations were likely due to macropore flow from voids beneath the DRIs. Other known sources that produce overestimation of measured infiltration rates using a DRI are separation of the soil from the wall of the DRI and lateral divergence. Lateral divergence can be caused by capillarity on adjacent soils, restrictive layers causing a perched water table and using too high of a pressure head (Bouwer 1986). The soils encountered below the gravelly fill were also relatively uniform. All material tested passed the #4 sieve (10mm) and no inclusions were discovered during excavation. However, extensive subsurface exploration was not performed before testing. Restrictive layers may have been present under the infiltrometers. Low heads were used during testing to try and avoid the third error source.

The measured rates varied over two orders of magnitude for the Lawrenceville site and one order of magnitude for the Covington site. However, this is not unexpected because in-situ values of hydraulic conductivity have been known to have a coefficient of variation as high as 800% (Reynolds et al. 2002). The results obtained in this study were within the bounds of variability found in literature.

From the very limited data collected, there seems to be poor correlation between NRCS and measured infiltration rates. The NRCS estimates did over predict the measured rates in every case. However, the estimates provided by the ROSETTA pedotransfer function both under and over predicted the measured rates. Much more data would need to be collected before evaluating the efficacy of either of these sources as reliable predictors.

4.9 Discussion – Hydraulic Conductivity of Binary Mixtures

In all cases, the hydraulic conductivity decreased with increasing silt content, as was expected. The observed decrease of two orders of magnitude agrees with the literature (Bandini et al. 2009; Sathees 2006; Thevanayagam and Martin 2000). However, the precipitous decrease in hydraulic conductivity at the estimated FC* of 17% was not observed; rather the conductivity decreased over one order of magnitude from 0 to 17% fines. Belkhatir et al. (2014) and Zhang et al. (2009) observed the same relationship with increasing silt content.

The measured hydraulic conductivity decreased with decreasing void ratio. This was also expected, as the void space available to contribute to conduction decreased as the increasing silt content filled the pores. The difference between hydraulic conductivities due to increased density of specimen was larger than what had observed in previous literature. For the 5% silt specimens, there was an 83% decrease in measured hydraulic conductivity between the loose and dense specimens. This can be compared with a 25% decrease observed in literature (Bandini et al. 2009; Sathees 2006) (B-value obtained for the loose and dense specimens was 0.95 and 0.96, respectively). The 5% loose specimen was somewhat under the target density. The target global void ratio to achieve a Dr of 20% was 0.78, and the actual global void ratio achieved was 0.82. This resulted is a lower than anticipated density relative to the rest of the specimens tested in a loose state. The difference between the remaining silt contents and densities were in better agreement with literature.

The intergranular void ratio increased as the silt content increased, and the hydraulic conductivity decreased as the intergranular void ratio and silt content increased. Sathees (2006) observed the same behavior for ASTM 50/50 sand mixed with Sil-Co-Sil

106. Belkhatir et al. (2014) observed a sharp, linear decrease in between 0 and 30% silt content with intergranular void ratio. Between 30 and 50% silt content, the increase was less pronounced (Belkhatir et al. 2014). Although this study did not test materials higher than the theoretical FC*, the trend in decreasing hydraulic conductivity between 0 and 17% was noticeably greater than the decrease from 17% to 100% silt for the densified specimens.

Generally, the hydraulic conductivity decreased with increasing confining stress, which was more pronounced with increases silt content. This is the opposite of what was found in literature (Bandini et al. 2009; Sathees 2006). There are three instances were an increase in hydraulic conductivity is observed. The pressure panel used for these specimens has pressure regulators that become unstable at pressures larger than 280 kPa. This may have caused spurious increases in hydraulic conductivities as the specimen was consolidated to higher confining stresses.

The measured minimum void ratios produced higher than expected void ratios for the sand-silt mixtures. While the expected minimum was observed at the estimated FC* of 17% silt content, the decrease did not exhibit the sharp decrease expected. Figure 4-12 and Figure 4-14 shows the variation in ideal packing, the theoretical lower bound, and the measured minimum void ratios. The coefficient from the Factional Packing model, y_{min}, was 0.46. This means that, per the Fractional Packing model there were only 46% of fines located in the voids of the coarser sand. The Mixing Coefficient model consistently under predicted the measured void ratios. The calculated λ_{avg} was 0.63. A λ value of 0.2 more closely predicts the measured minimum void ratios. A λ value of 0 and 1 imply zero mixing and ideal mixing, respectively. However, the Mixing Coefficient Model was

developed, and λ_{avg} was obtained through regression of glass beads of varying size. The designation of gravel and sand was assigned based on the diameters of the beads (Zhang et al. 2009). The uniformity of glass bead results in differing packing efficiencies than that of sand and silt mixtures (Cho et al. 2006; McGeary 1961).

The parabolic shape of the predicted void ratios yielded from the Fractional Packing model is a mathematical artifact. Kamann et al. (2007) observed that the equation for the coarse packing region can be substituted into the corresponding porosity equation to show that porosity is a parabolic function of c, the volume fraction of fines. The first and second derivatives show that the minimum will occur at:

$$c = 0.5\phi_c\left(\phi_f - 1\right)\left(\phi_f - \phi_{min}{\phi_c}^{-1}\right)^{-1}$$

When this minimum occurs at values of c less than the porosity of the coarse fraction a false minimum occurs (Kamann et al. 2007).

The measured maximum void ratios are more closely predicted by the Fractional Packing model and Mixing Coefficient model up to the 10% silt contents. The higher silt contents begin to diverge from the predicted value toward the upper bound estimate.

The Mixing Coefficient model takes into account changing porosity and representative grain size diameter as the fines content changes. The predicted saturated hydraulic conductivities were consistently higher than the measured values for both densities, regardless of the accuracy of the porosity, or void ratio, prediction. The trend of decreasing conductivity with increasing silt content is captured up to the FC*. However, the measured hydraulic conductivity for 100% Sil-Co-Sil 40 differ from the predicted by two orders of magnitude. None of the predictive models reviewed consider specific surface with regard to the hydraulic conductivity of fine grained material (material

passing the #200 sieve for the USCS), and hydraulic conductivity of fine grained soils is dependent on specific surface in addition to viscous drag, void ratio and tortuosity (Santamarina et al. 2002).

Chapter 5

CONCLUSION

In this study, the infiltration rates were measured in-situ at two sites in the Piedmont physiographic province of Georgia. The efficacy of predicting saturated hydraulic conductivity for Piedmont soils via published soil surveys from the National Resource Conservation Service and pedotransfer functions was investigated. Constant head methods were employed using a double-ring infiltrometers with Mariotte tubes to maintain the head. The soils encountered in-situ ranged from sandy soils to silts to clays. Laboratory based measurements of the saturated hydraulic conductivity of binary mixtures to investigate the effects of particle mixtures on hydraulic conductivity. The materials used were ASTM 100/200 sand and Sil-Co-Sil 40 non-plastic silt. The materials were chosen based on the ratio of the mean particle diameters. Two fixed densities were used to investigate the effects of particle packing on the hydraulic conductivity of binary mixtures. The critical fines content where the finer particles completely fill the pore volume of the coarse particles was predicted. Incremental fines contents, by mass, up to this theoretical fines content were tested. The measured saturated hydraulic conductivity was evaluated in terms of fines content, global and intergranular void ratio, and confining stress. Models for predicting extreme void ratios and saturated hydraulic conductivity of binary mixtures were also investigated.

The major findings of this study include:

- Predicted values from the NRCS over predicted every measured value of in-situ saturated hydraulic conductivity.

- Predicted values from the ROSETTA pedotransfer software predicted the saturated hydraulic conductivity with reasonable accuracy.
- Saturated hydraulic conductivity of the sand/silt mixture decreased by two orders of magnitude with the introduction of the silt up to the estimated critical fines content of 17%.
- The rate of decrease diminished for specimens prepared with silt content greater than the critical fines content.
- Decreases in saturated hydraulic conductivity with increasing density, or decreasing global void ratio, were greater in specimens containing more than 1% silt.
- The saturated hydraulic conductivity deceased with decreasing global void ratio and increasing intergranular void ratio.
- Predictive models for extreme void ratios of binary mixtures consistently under predicted the measured void ratios.
- Predictive models for saturated hydraulic conductivity consistently over predicted measured rates.

APPENDIX A

The Atterberg Limits were determined using method BS 1377. The correlation proposed by Feng (2004) was used to calculate the plastic limit.

$$PL = C(2)^m$$

The LL, PL, PI. Feng (2004) parameters, and USCS soil types are summarized in Table A-1. Figures A-1, A-2, A-3, A-4, A-5 and A-6 show the water content with penetration depth, and Figure A-7 shows the plasticity chart used to classify the fine grained soils.

Table A-1 Summary of Atterberg Limits and Soil Types per USCS

Test Pit	LL	C	m	PL	PI	USCS	Group Name
TPC2	53.0	20.730	0.372	26.8	26.2	CH	Sandy Fat Clay
TPC3	59.5	27.490	0.258	32.9	26.6	MH	Sandy Elastic Silt
TPL1	45.0	19.510	0.345	24.8	20.2	CL	Sandy Clay
TPL2	52.0	22.860	0.335	28.8	23.2	CH	Sandy Fat Clay
TPL3	50.0	20.249	0.359	26.0	24.0	SC	Clayey Sand
TPL4	60.0	20.458	0.406	27.1	32.9	CH	Sandy Fat Clay

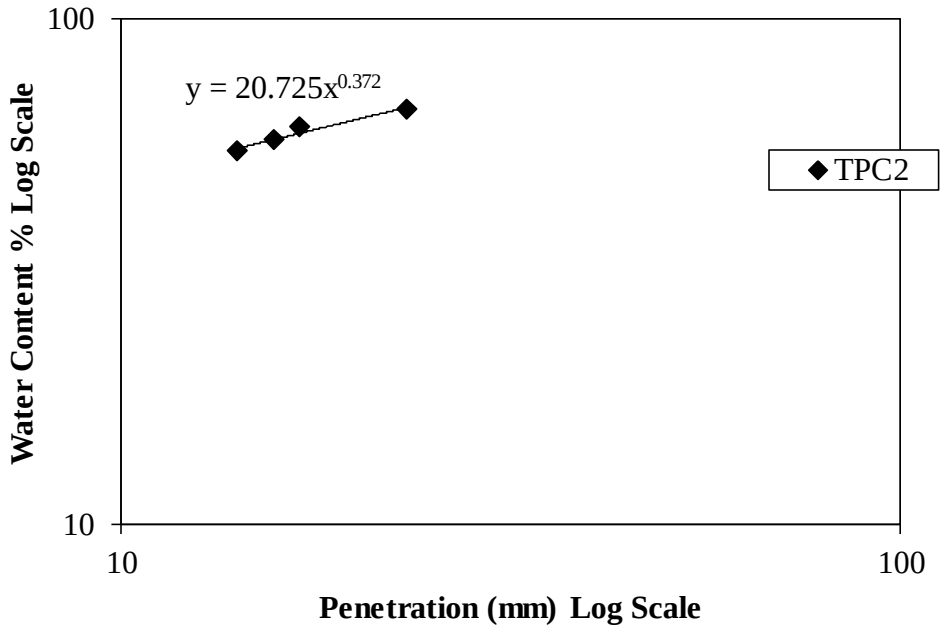

Figure A-1 Liquid and Plastic Limit were determined by method BS 1377 for TPC2.

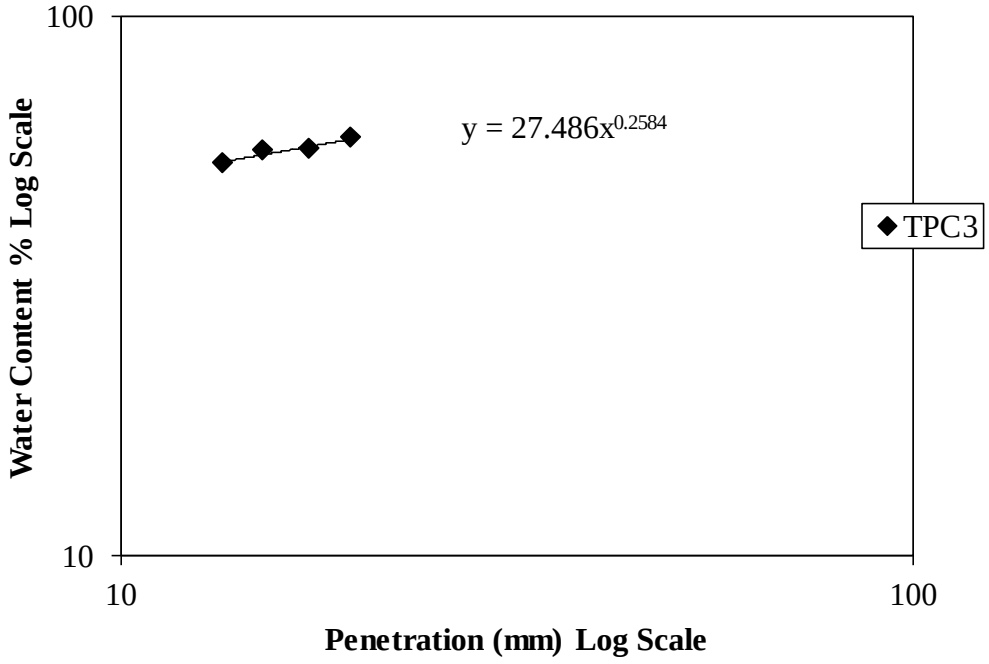

Figure A-2 Liquid and Plastic Limit were determined by method BS 1377 for TPC3.

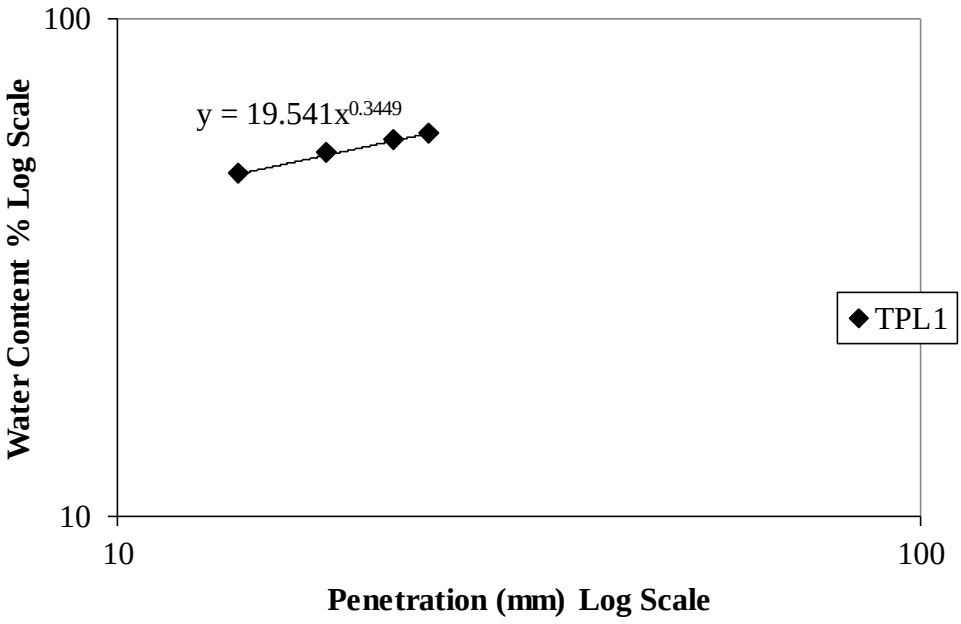

Figure A-3 Liquid and Plastic Limit were determined by method BS 1377 for TPL1.

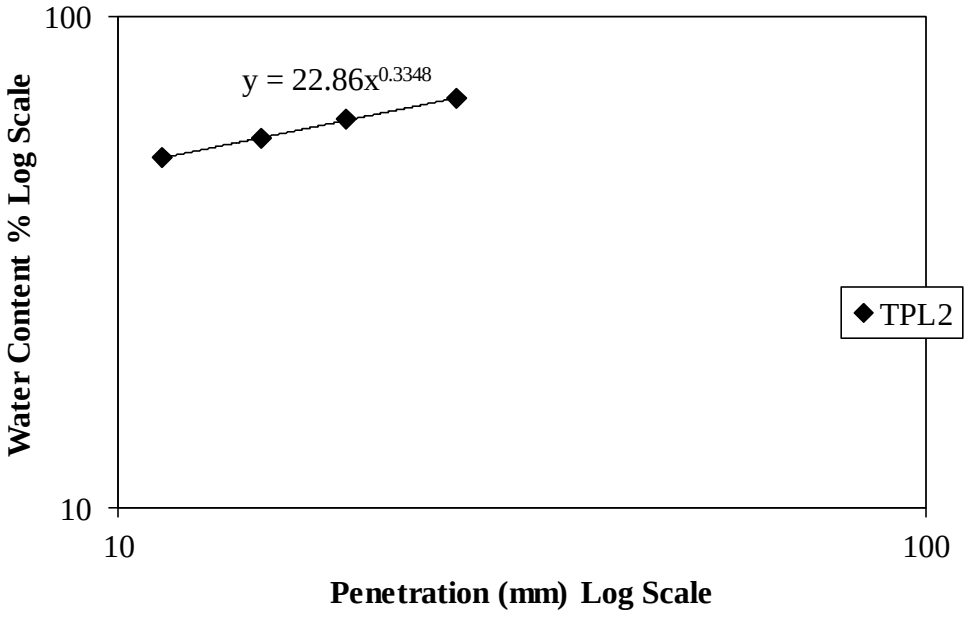

Figure A-4 Liquid and Plastic Limit were determined by method BS 1377 for TPL2.

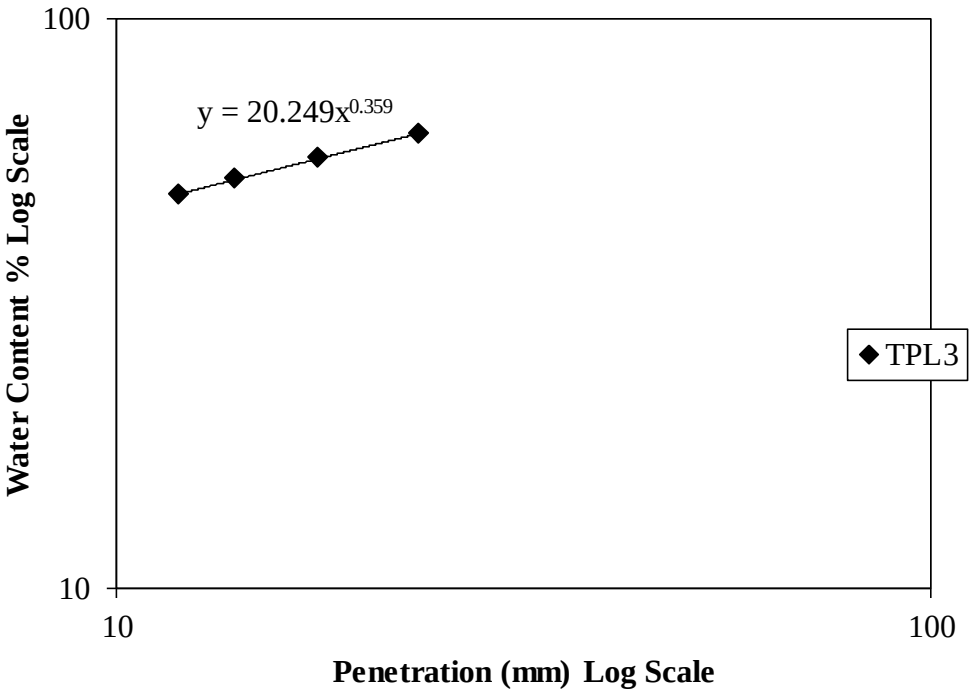

Figure A-5 Liquid and Plastic Limit were determined by method BS 1377 for TPL3.

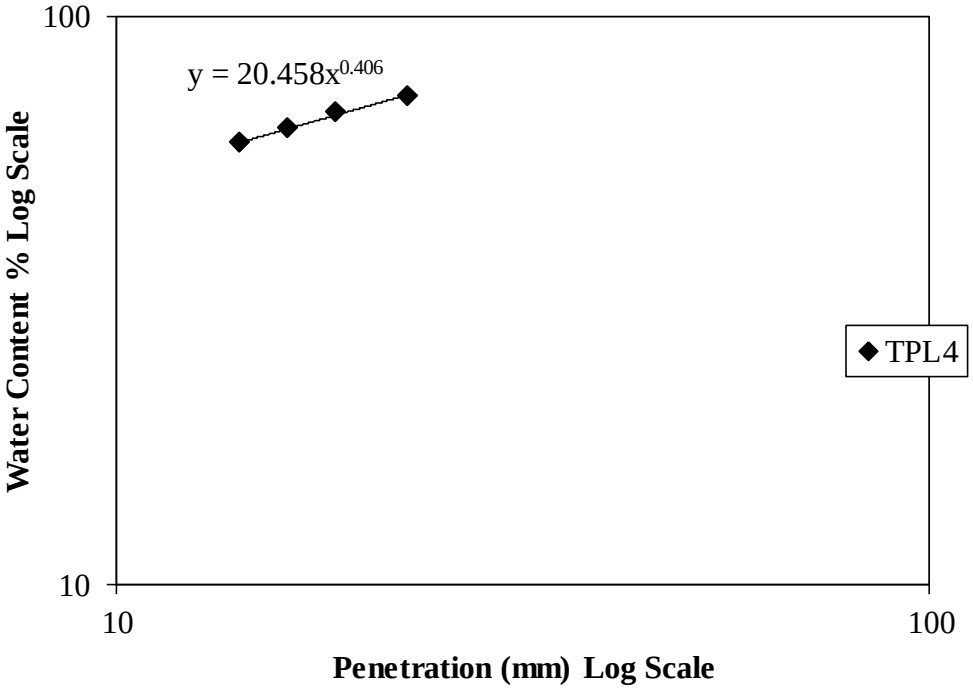

Figure A-6 Liquid and Plastic Limit were determined by method BS 1377 for TPL4.

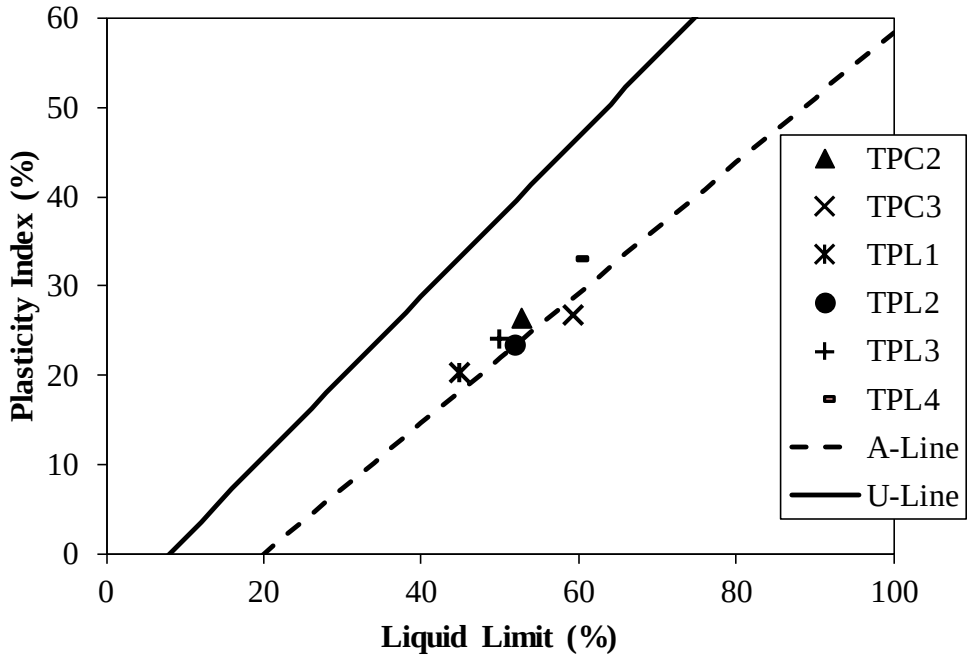

Figure A-7 The measured liquid limits and plasticity indices are shown on the plasticity chart.

APPENDIX B

The minimum and maximum void ratios were measured using methods described in ASTM D4253 and ASTM D4254. Methods 1A and C were used, respectively. Tables B-1 and B-2 show the measured values. The 100% Sil-Co-Sil 40 values were measured by Dr. Hyunwook Choo. The saturated hydraulic conductivity with fines content and confining pressure are shown in Table B-3 and B-4. Tables B-5 and B-6 contain the fines content, void ratios and intergranular void ratios.

Table B-1 Minimum Void Ratios for Sand/Silt Mixture

Minimum Void Ratio				
Mixture	Trials			Average
	1	2	3	
0	0.550	0.559	0.589	0.566
1	0.536	0.576	0.549	0.554
5	0.541	0.551	0.555	0.549
10	0.540	0.547	0.546	0.544
17	0.503	0.513	0.518	0.512
100	N/A	N/A	N/A	0.640

Table B-2 Maximum Void Ratios for Sand/Silt Mixture

Maximum Void Ratio						
Mixture	Trials					Average
	1	2	3	4	5	
0	0.850	0.867	0.850	0.867	0.867	0.860
1	0.874	0.839	0.839	0.857	0.839	0.850
5	0.821	0.857	0.821	0.821	0.857	0.836
10	0.785	0.821	0.785	0.821	0.821	0.806
17	0.846	0.828	0.828	0.846	0.828	0.835
35	1.077	1.121	1.121	1.121	1.099	1.108
100	N/A	N/A	N/A	N/A	N/A	1.810

Table B-3 k_{sat} with Confining Stress for the Loosely Prepared Specimens

k_{sat} (cm/s) for Loose Specimens (Dr ~ 20%)						
Confining Stress (kPa)	Fines Content by Mass (%)					
	0	1	5	10	17	100
35	2.0E-03	1.0E-03	5.8E-04	3.9E-04	1.1E-04	8.5E-06
70	2.0E-03	9.1E-04	3.4E-04	2.6E-04	1.0E-04	8.1E-06
105	1.9E-03	8.5E-04	2.8E-04	Terminated	9.5E-05	7.1E-06
140	1.8E-03	7.3E-04	3.1E-04	Terminated	8.9E-05	6.1E-06

Table B-4 k_{sat} with Confining Stress for the Densely Prepared Specimens

k_{sat} (cm/s) for Dense Specimens (Dr ~ 70%)						
Confining Stress (kPa)	Fines Content by Mass (5)					
	0	1	5	10	17	100
35	1.3E-03	1.0E-03	9.7E-05	8.8E-05	5.1E-05	8.5E-06
70	1.4E-03	9.2E-04	1.1E-04	8.3E-05	4.6E-05	8.1E-06
105	1.4E-03	7.6E-04	8.6E-05	7.2E-05	3.6E-05	7.1E-06
140	9.0E-04	9.2E-04	8.5E-05	7.6E-05	3.3E-05	6.1E-06

Table B-5 Target and Measured Values for Fines Content and Global Void Ratio for Loosely Prepared Specimens

Loose (Dr ~ 20%)					
Target Fines Content (%)	Actual Fines Content (%)	k_{sat} (cm/s)	Initial Global Void Ratio, e_o	Target Global Void Ratio, e	Intergranular Void Ratio, e_s
0	0	2.2E-03	0.820	0.802	0.820
1	N/A	1.0E-03	0.790	0.791	0.808
5	5.7	5.8E-04	0.820	0.778	0.916
10	10.1	3.9E-04	0.760	0.754	0.956
17	17.5	1.1E-04	0.730	0.770	1.084
100	100.0	8.5E-06	0.970	N/A	N/A

Table B-6 Target and Measured Values for Fines Content and Global Void Ratio for Densely Prepared Specimens

Dense (Dr ~ 70%)					
Target Fines Content (%)	Actual Fines Content (%)	k_{sat} (cm/s)	Initial Global Void Ratio, e_o	Target Global Void Ratio, e	Intergranular Void Ratio, e_s
0	0	1.3E-03	0.660	0.654	0.660
1	1.2	9.0E-04	0.640	0.643	0.657
5	5.2	1.0E-04	0.630	0.635	0.716
10	11.0	8.8E-05	0.650	0.623	0.833
17	17.0	5.1E-05	0.580	0.607	0.904
100	100	8.5E-06	0.970	N/A	N/A

REFERENCES

Arriaga, F. J., Kornecki, T. S., Balkcom, K. S., and Raper, R. L. (2010). "A method for automating data collection from a double-ring infiltrometer under falling head conditions." *Soil Use and Management*, 26(1), 61–67.

Arrington, K. E., Ventura, S. J., and Norman, J. M. (2013). "Predicting Saturated Hydraulic Conductivity for Estimating Maximum Soil Infiltration Rates." *Soil Science Society of America Journal*, 77(3), 748.

Bandini, P., Asce, M., and Sathiskumar, S. (2009). "Effects of Silt Content and Void Ratio on the Saturated Hydraulic Conductivity and Compressibility of Sand-Silt Mixtures." *Journal of Geotechnical and Geoenvironmental Engineering*, 135(12), 1976–1980.

Barbu, I. A., and Ballestero, T. P. (2014). "Unsaturated Flow Functions for Filter Media Used in Low-Impact Development — Stormwater Management Systems." *Journal of Irrigation and Drainage*, 1–11.

Bedient, P. B., Huber, W. C., and Baxter, E. V. (2013). *Hydrology and Floodplain Analysis*. (H. Stark, C. Heinle, and S. Disanno, eds.), Pearson, Upper Saddle River, NJ.

Belkhatir, M., Arab, A., Della, N., and Schanz, T. (2014). "Laboratory Study on the Hydraulic Conductivity and Pore Pressure of Sand-Silt Mixtures." *Marine Georesources & Geotechnology*, 32(2), 106–122.

Bouwer, H. (1986). "Intake Rate: Cylinder Infiltrometers." *Methods of Soil Analysis, Part 1: Physical and Mineralogical Methods*, American Society of Agronomy and Soil Science Society of America, Madison, Wiscosin, 825–844.

Bouwer, H., and Rice, R. C. (1976). "A slug test for determining hydraulic conductivity of unconfined aquifers with completely or partially penetrating wells." *Water Resources Research*, 12(3), 423–428.

Bouwer, H., and Rice, R. C. (1984). "Hydraulic Properties of Stony Vadose Zones." *Groundwater*, 22(6), 696 – 705.

Brown, D. L., Narasimhan, T. N., and Demir, Z. (1995). "An evaluation of the Bouwer and Rice method of slug test analysis." *Water Resource Research*, 31(5), 1239–1246.

Carraro, J. A. H., Asce, S. M., Bandini, P., Salgado, R., and Asce, M. (2003). "Liquefaction Resistance of Clean and Nonplastic Silty Sands Based on Cone

Penetration Resistance." *Journal of Geotechnical and Geoenvironmental Engineering*, American Society of Civil Engineers, Austin, 965–976.

Castelbaum, D., and Shackelford, C. D. (2010). "Hydraulic Conductivity of Bentonite Slurry Mixed Sands." 135(12), 1941–1956.

Chen, J. S., Ouyang, Y., Ravi, V., and Williams, J. R. (1998). *Estimation of Infiltration Rate in the Vadose Zone: Application of Selected Mathematical Models Volume II*. Washington, DC.

Cho, G. C., and Santamarina, J. C. (2001). "Unsaturated Particulate Materials - Particle Level Studies." *Geotechnical and Geotenvironmental Engineering*, 127(1), 84–96.

Cho, G.-C., Dodds, J., and Santamarina, J. C. (2006). "Particle Shape Effects on Packing Density, Stiffness, and Strength: Natural and Crushed Sands." *Journal of Geotechnical and Geoenvironmental Engineering*, 132(5), 591–602.

Choo, H., and Burns, S. E. (2014). "Effect of overconsolidation ratio on dynamic properties of binary mixtures of silica particles." *Soil Dynamics and Earthquake Engineering*, Elsevier, 60, 44–50.

Dingman, S. L. (2008). *Physical Hydrology*. Waveland Press, Inc, Long Grove, IL.

Ellington, M. M., and Ferguson, B. K. (1991). "COMPARISON OF INFILTRATION AND DETENTION IN THE GEORGIA PIEDMONT USING RECENT HYDROLOGIC MODELS." *1991 Georgia Water Resources Conference*, Athens, GA, 213–216.

Estes, C. J. (2007). "Storm Water Infiltration in Clay Soils : A Case Study of Storm Water Retention and Infiltration Techniques in The North Carolina Piedmont." *2nd National Low Impact Development Conference*, ASCE, 159–170.

Fedler, C. B., Littlejohn, J., Duan, R., and Feng, L. (2012). *TCEQ Report No. 582-9-90350: Refining the Application Rates for Onsite Surface Application*. Lubbock, TX.

Feng, T. (2004). "Using a Small Ring and a Fall-Cone to Determine the Plastic Limit." *Journal of Geotechnical and Geoenvironmental Engineering*, 130(6), 630–635.

Ferguson, B. K. (1994). *Stormwater Infiltration*. CRC Press, Inc, Boca Raton, Florida.

Finke, K. A., Mayne, P. W., and Klopp, R. A. (2001). "Piezocone Penetration Testing in Atlantic Piedmont Residuum." *Journal of Geotechnical and Geoenvironmental Engineering*, 127(January), 48–54.

Frost, J. D., and Park, J. Y. (2003). "A Critical Assessment of the Moist Tamping Technique." *Geotechnical Testing Journal*, 26(1), 1–14.

Fuggle, A. R. (2011). "GEOMATERIAL GRADATION INFLUENCES ON INTERFACE SHEAR BEHAVIOR." Georgia Institute of Technology.

Furnas, C. C. (1929). *Flow of Gases Through Broken Solids*. Washington, DC.

Furnas, C. C. (1931). "Grading Aggregates I - Mathematical Relations for Beds of Broken Soilds of Maximum Density." *Industrial and Engineering Chemistry*, 23(9), 1052–1058.

Genuchten, M. T. Van. (1980). "Closed-form Equation for Predicting the Hydraulic Conductivity of Unsaturated Soils, A." *Soil Science Society of America Journal*, 44(8), 892–898.

Gorelick, S. M., and Koltermann, C. E. (1995). "Fractional packing model for hydraulic conductivity derived from sediment mixture." *Water Resource Research*, 31(12), 3283–3297.

Gregory, J. H., Dukes, M. D., Jones, P. H., and Miller, G. L. (2006). "Effect of urban soil compaction on." *Journal of Soil and Water Conservation*, 61(3), 117–124.

Hsu, S. M., Asce, M., Ni, C., and Hung, P. (2002). "Assessment of Three Infiltration Formulas based on Model Fitting on Richards Equation." *Journal of Hydrologic Engineering*, 7(5), 373–379.

Kamann, P. J., Ritzi, R. W., Dominic, D. F., and Conrad, C. M. (2007). "Porosity and permeability in sediment mixtures." *Ground water*, 45(4), 429–38.

Komine, H. (2010). "Predicting hydraulic conductivity of sand–bentonite mixture backfill before and after swelling deformation for underground disposal of radioactive wastes." *Engineering Geology*, Elsevier B.V., 114(3-4), 123–134.

Kuerbis, R., and Vaid, Y. P. (1988). "Sand Sample Preparation - The Slurry Deposition Method." *Soils and Foundations*, 28(4), 107 – 118.

Ladd, R. S. (1978). "Preparing Test Specimens Using Undercompaction." *Geotechnical Testing Journal*, 1(1), 16–23.

Lade, P. V., Liggio, C. D., and Yamamuro, J. A. (1998). "Effects of Non-Plastic Fines on Minimum and Maximum Void Ratios of Sand." *Geotechnical Testing Journal*, 21(4), 336–347.

Lai, J., Luo, Y., and Ren, L. (2010). "Buffer Index Effects on Hydraulic Conductivity Measurements Using Numerical Simulations of Double-Ring Infiltration." *Soil Science Society of America Journal*, 74(5), 1526.

Lai, J., Luo, Y., and Ren, L. (2012). "Numerical Evaluation of Depth Effects of Double-Ring Infiltrometers on Soil Saturated Hydraulic Conductivity Measurements." *Soil Science Society of America Journal*, 76(3), 867.

Lai, J., and Ren, L. (2007). "Assessing the Size Dependency of Measured Hydraulic Conductivity Using Double-Ring Infiltrometers and Numerical Simulation." *Soil Science Society of America Journal*, 71(6), 1667.

Lu, N., and Likos, W. J. (2004). *Unsaturated Soil Mechanics*. John Wiley and Sons Ltd, Hoboken, New Jersey.

Massman, J. W. (2003). "A Design Manual for Sizing Infiltration Ponds." *Washington State Department of Trasportation*, (October).

McGeary, R. K. (1961). "Mechanical Packing of Spherical Particles." *Journal of The American Ceramic Society*, 44(10), 513 – 522.

Palomino, A. M., Burns, S. E., and Santamarina, J. C. (2008). "Mixtures of fine-grained minerals – kaolinite and carbonate grains." *Clays and Clay Minerals*, 56(6), 599–611.

Philips, E. C., and Kitch, W. A. (2011). "A review of methods for characterization of site infiltration with design recommendations." *43rd Symposium on Engineering Geology and Geotechnical Engineering*, Las Vegas, NV, 23–25.

Phillips, P. M. (2007). "POROSITY AND PERMEABILITY OF BIMODAL SEDIMENT MIXTURES USING NATURAL SEDIMENT." Wright State University.

Rawls, W. J., Brakensiek, D. L., and Miller, N. (1983). "Green-ampt Infiltration Parameters from Soils Data." *Journal of Hydraulic Engineering*, 109(1), 62–70.

Rawls, W. J., Brakensiek, D. L., and Saxton, K. E. (1982). "Estimation of Soil Water Properties." *American Society of Agricultural Engineers*, 25(5), 1316 – 1330.

Rawls, W. J., Saxton, K. E., and Brakensiek, D. L. (1982). "Estimation of Soil Water Properties." *American Society of Agricultural Engineers*, 25(5), 1316–1320.

Reynolds, W. D. (2013). "An assessment of borehole infiltration analyses for measuring field-saturated hydraulic conductivity in the vadose zone." *Engineering Geology*, Elsevier B.V., 159, 119–130.

Reynolds, W. D., Elrick, D. E., Youns, E. G., Amoozegar, A., Booltink, H. W. G., and Bouma, J. (2002). "Saturated and Field Saturated Water Flow Parameters." *Methods of Soil Analysis: Part 4 - Physical Methods*, J. H. Dane and G. C. Topp, eds., Soil Science Society of America, Inc, Madison, Wiscosin, 797 – 877.

Santamarina, J. C., and Fratta, D. (2005). *Discrete Signals and Inverse Problems: An Introduction for Engineers and Scientists*. John Wiley and Sons Ltd, West Sussex.

Santamarina, J. C., and Jang, J. (2010). "Energy geotechnology : Implications of mixed fluid conditions." *5th International Conference on Unsaturated Soils*, A. Gens and E. Alonso, eds., Barcelona.

Santamarina, J. C., Klein, K. A., and Fam, M. A. (2001). *Soils and Waves Particulate Materials Behavior, Characterization and Process Monitoring*. John Wiley and Sons Ltd, West Sussex.

Santamarina, J. C., Klein, K. A., Wang, Y. H., and Prencke, E. (2002). "Specific surface : determination and relevance." *Canadian Geotechnical Journal*, 241, 233–241.

Sathees, T. (2006). "Saturated hydraulic conductivity of poorly graded sands with non-plastic silts using a flexible wall permeameter." New Mexico State University.

Saxton, K. E., and Rawls, W. J. (2006). "Soil Water Characteristic Estimates by Texture and Organic Matter for Hydrologic Solutions." *Soil Science Society of America Journal*, 70(5), 1569.

Schaap, M. G., Leij, F. J., and van Genuchten, M. T. (2001). "Rosetta: a Computer Program for Estimating Soil Hydraulic Parameters With Hierarchical Pedotransfer Functions." *Journal of Hydrology*, 251(3-4), 163–176.

Sivapullaiah, P. V., Sridharan, a., and Stalin, V. K. (2000). "Hydraulic conductivity of bentonite-sand mixtures." *Canadian Geotechnical Journal*, 37(2), 406–413.

Stewart, J. W. (1964). *Infiltration and Permeability of Weathered Crystalline Rocks Georgia Nuclear Laboratory Dawson County, Georgia - Studies of Sites for Nuclear Energy Facilities*. Dawson County, GA.

Thevanayagam, S. (1998). "EFFECT OF FINES AND CONFINING STRESS ON UNDRAINED SHEAR." *Journal of Geotechnical and Geoenvironmental Engineering*, 124(6), 479–491.

Thevanayagam, S., and Martin, G. R. (2000). "Liquifaction in silty soils - screening and remediation issues." *International Workshop on Mitigation of Seismic Effects on Transportation Structures*, National Center for Research on Earthquake Engineering, Taipei, Taiwan.

Thevanayagam, S., Shenthan, T., Mohan, S., and Liang, J. (2002). "Undrained Fragility of Clean Sands , Silty Sands , and Sandy Silts." *Journal of Geotechnical and Geoenvironmental Engineering*, 128(10), 849–859.

Urso, M., Lawrence, C., and Adams, M. (1999). "Pendular, Funicular, and Capillary Bridges: Results for Two Dimensions." *Journal of colloid and interface science*, 220(1), 42–56.

WEF, ASCE, and EWRI. (2012). "Infiltrators." *Design of Urban Stormwater Controls*, McGraw Hill, Alexandria and Reston, Virginia.

Wood, F. M., Yamamuro, J. a., and Lade, P. V. (2008). "Effect of depositional method on the undrained response of silty sand." *Canadian Geotechnical Journal*, 45(11), 1525–1537.

Wösten, J. H. M., Pachepsky, Y. A., and Rawls, W. J. (2001). "Pedotransfer functions: bridging the gap between available basic soil data and missing soil hydraulic characteristics." *Journal of Hydrology*, 251(3-4), 123–150.

Yang, S., Lacasse, S., and Sandven, R. (2006). "Determination of the Transitional Fines Content of Mixtures of Sand and Non-plastic Fines." *Geotechnical Testing Journal*, 29(2), 3–8.

Yeo, S., Shackelford, C. D., and Evans, J. C. (2006). "Consolidation and Hydraulic Conductivity of Nine Model Soil-Bentonite Backfills." 131(10), 1189–1198.

Zhang, Z. F., Ward, A. L., and Keller, J. M. (2009). *Determining the Porosity and Saturated Hydraulic Conductivity of Binary Mixtures*. Richland, Washington.

Zornberg, J. G., Asce, M., Mccartney, J. S., and Asce, A. M. (2010). "Centrifuge Permeameter for Unsaturated Soils . I : Theoretical Basis and Experimental Developments." *Journal of Geotechnical and Geoenvironmental Engineering*, 136(8), 1051–1063.